Article

Developmental Cell

Global Proteome Remodeling during ER Stress Involves Hac1-Driven Expression of Long Undecoded Transcript Isoforms

Graphical Abstract

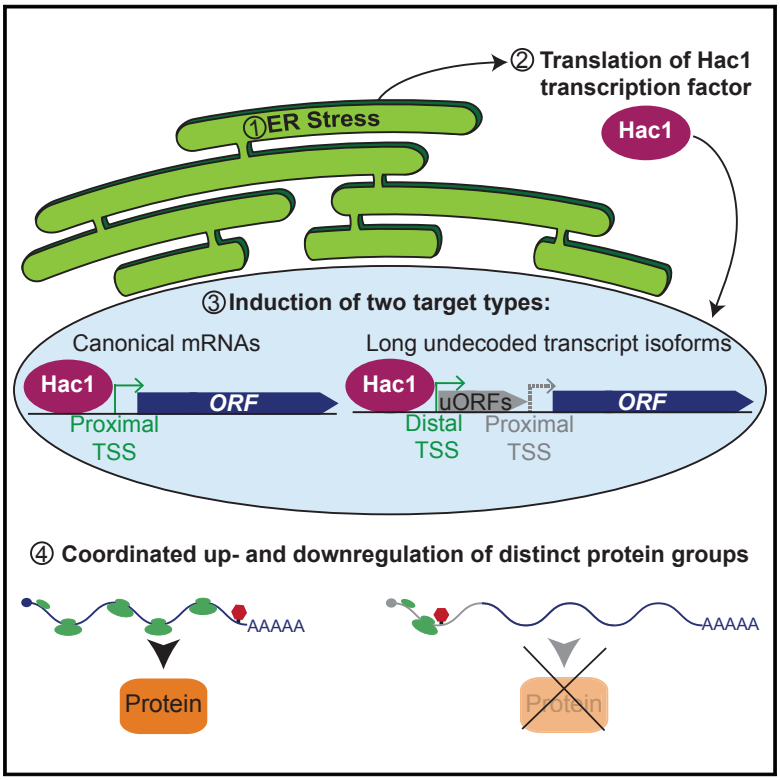

Authors

Kelsey Marie Van Dalfsen, Stefanie Hodapp, Abdurrahman Keskin, ..., Daniel Koji Nomura, Marko Jovanovic, Gloria Ann Brar

Correspondence

gabrar@berkeley.edu

In Brief

Van Dalfsen et al. demonstrate that conserved yeast transcription factor Hac1/XBP1 directs the ER unfolded protein response (UPR^{ER}) by not only gene activation but also coordinated gene repression through a mechanism of long undecoded transcript isoform (LUTI) production. Via the LUTI mechanism, Hac1 mediates proteome remodeling and influences cellular metabolism control.

Highlights

- Yeast Hac1/XBP1 coordinates up- and downregulation of distinct protein sets during the UPR^{ER}
- Repression occurs via induction of long undecoded transcript isoforms (LUTIs)
- Hac1 directs proteome and metabolic remodeling as part of the UPR^{ER}
- Reducing cellular respiration improves fitness of UPR^{ER}-activated cells

Van Dalfsen et al., 2018, Developmental Cell *46*, 219–235
July 16, 2018
https://doi.org/10.1016/j.devcel.2018.06.016

CellPress

Developmental Cell
Article

Global Proteome Remodeling during ER Stress Involves Hac1-Driven Expression of Long Undecoded Transcript Isoforms

Kelsey Marie Van Dalfsen,[1] Stefanie Hodapp,[2] Abdurrahman Keskin,[2] George Maxwell Otto,[1] Charles Andrew Berdan,[3] Andrea Higdon,[1] Tia Cheunkarndee,[1] Daniel Koji Nomura,[1,3] Marko Jovanovic,[2] and Gloria Ann Brar[1,4,*]
[1]Department of Molecular and Cell Biology, University of California, Berkeley, CA 94720, USA
[2]Department of Biological Sciences, Columbia University, New York, NY 10027, USA
[3]Departments of Chemistry and Nutritional Sciences and Toxicology, University of California, Berkeley, CA 94720, USA
[4]Lead Contact
*Correspondence: gabrar@berkeley.edu
https://doi.org/10.1016/j.devcel.2018.06.016

SUMMARY

Cellular stress responses often require transcription-based activation of gene expression to promote cellular adaptation. Whether general mechanisms exist for stress-responsive gene downregulation is less clear. A recently defined mechanism enables both up- and downregulation of protein levels for distinct gene sets by the same transcription factor via coordinated induction of canonical mRNAs and long undecoded transcript isoforms (LUTIs). We analyzed parallel gene expression datasets to determine whether this mechanism contributes to the conserved Hac1-driven branch of the unfolded protein response (UPR^{ER}), indeed observing Hac1-dependent protein downregulation accompanying the upregulation of ER-related proteins that typifies UPR^{ER} activation. Proteins downregulated by Hac1-driven LUTIs include those with electron transport chain (ETC) function. Abrogated ETC function improves the fitness of UPR^{ER}-activated cells, suggesting functional importance to this regulation. We conclude that the UPR^{ER} drives large-scale proteome remodeling, including coordinated up- and downregulation of distinct protein classes, which is partly mediated by Hac1-induced LUTIs.

INTRODUCTION

Gene regulatory programs are key drivers of cellular state change. The most common class of such programs are transcriptional, in which one or a few transcription factors (TFs) are activated in response to an environmental or developmental cue to induce expression of genes whose protein products are required to promote the transition to a new cell state. It seems likely that such cellular transitions should also require downregulation of gene sets, either because specific proteins impede the cell's transition to a new cellular state or simply for the cell to free up capacity for the production of proteins needed for the transition. The mechanisms by which such downregulation is achieved have been less well studied than those that drive upregulation, although some such mechanisms are known, including those involving protein degradation and transcriptional repressor proteins. With few exceptions (e.g., Haghighat et al., 1996; Hinnebusch, 1993; Hollien et al., 2009), however, our understanding of the gene regulatory programs underlying cellular state change has lacked a coherent explanation for how up- and downregulation are coordinated.

A recently defined mode of gene regulation is an attractive candidate for broadly mediating such coordination (Figure 1A). This mechanism was shown to harness TF-driven synthesis of an open reading frame (ORF)-encoding transcript to repress synthesis of the kinetochore protein Ndc80, a key event during meiotic differentiation in budding yeast (Chen et al., 2017; Chia et al., 2017). In short, it was found that *NDC80* has two transcription start sites (TSSs) that are activated by different TFs. Activation of the proximal TSS produces a canonical transcript that is translated to produce protein. Activation of the distal TSS results in synthesis of a 5′ extended transcript that encodes the *NDC80* ORF, but does not lead to ORF expression because of translation of upstream ORFs (uORFs) in the extended 5′ leader. Use of the distal TSS also represses use of the proximal TSS in *cis* by transcriptional interference. Effectively, as a result of this integrated mechanism, synthesis of the longer transcript halts Ndc80 protein production. This longer mRNA was termed a LUTI (long undecoded transcript isoform) (Chen et al., 2017; Chia et al., 2017).

Subsets of the hallmarks of LUTI-based regulation defined above were previously observed for several other genes (Law et al., 2005; Moseley et al., 2002; Sehgal et al., 2008), suggesting that use of this mechanism might be widespread. We recently found that LUTI-based regulation is common and responsible for setting protein levels of at least 380 genes as yeast cells progress through meiotic differentiation (Cheng et al., 2018). We showed that this mechanism enables a single meiotic TF to regulate two distinct sets of targets in a highly coordinated manner. The canonical set includes "positive" targets, whose transcription results in increased protein production, and "negative" LUTI targets, whose transcription leads to decreased protein production. While both sets of targets may exhibit increases in mRNA production, for genes that are regulated by the LUTI-based mechanism, overall mRNA levels are decoupled from

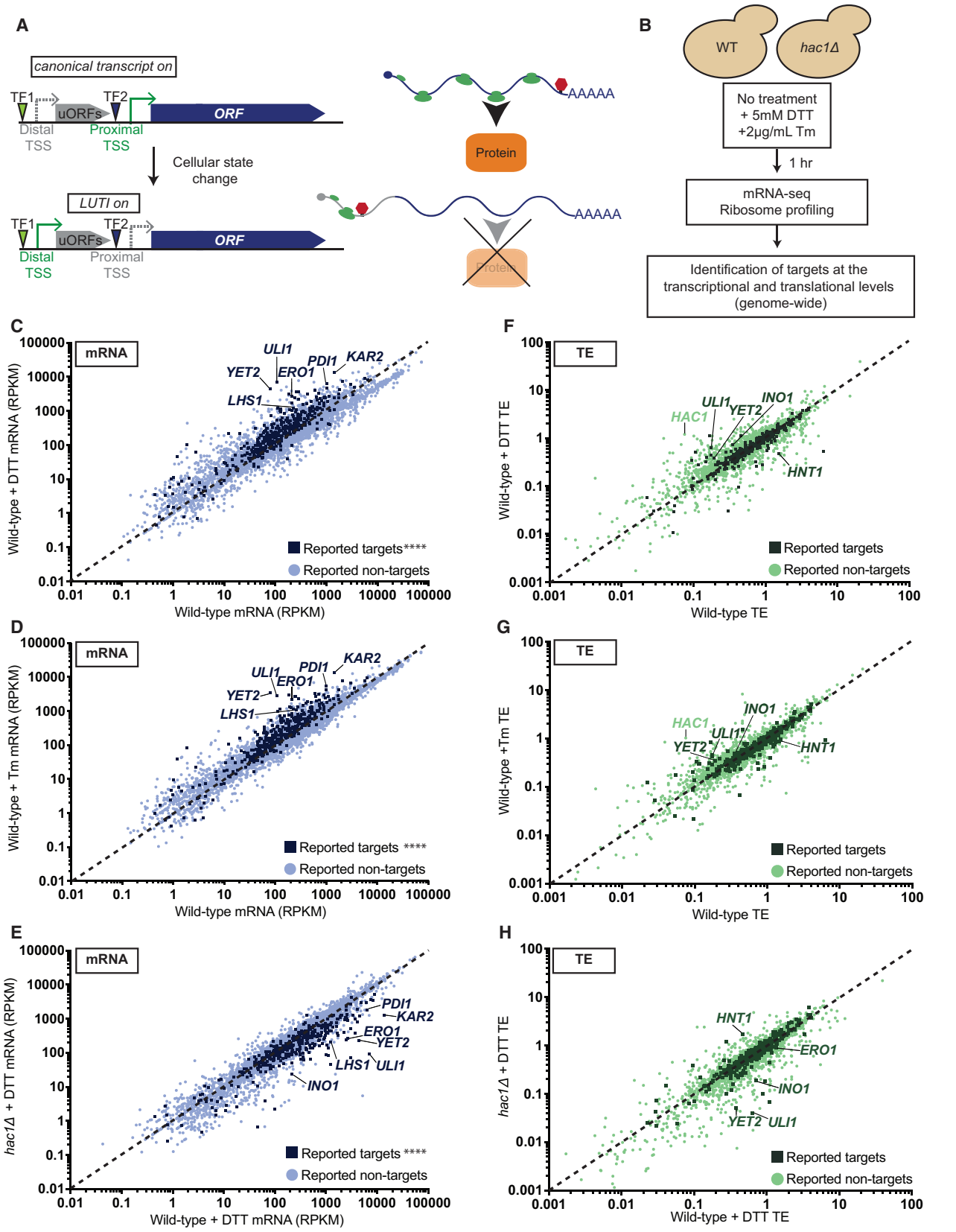

(legend on next page)

protein levels. In fact, the 380 meiotic LUTI targets that we defined were found based on the signature of a poor, or even negative, correlation between mRNA and protein levels over time (Cheng et al., 2018; Otto and Brar, 2018). For these cases, it is the type of transcript produced rather than the amount that determines whether protein is synthesized.

Given the pervasiveness of LUTI-based regulation during meiosis, it seemed possible that this mechanism might generally be used to coordinate gene up- and downregulation during cellular transitions. We sought a well-defined cellular state change in which to test this hypothesis. We chose to focus on the branch of the ER unfolded protein response (UPR^{ER}) that is conserved from budding yeast to human and relies on the Hac1 TF (orthologous to Xbp1 in metazoans) to allow cells to respond to aberrant protein folding within the ER lumen (reviewed in Han and Kaufman, 2017; Walter and Ron, 2011). The UPR^{ER} is typically experimentally induced by treatment of cells with drugs that disrupt ER folding, such as DTT or tunicamycin (Tm). The resulting accumulation of misfolded proteins in the ER lumen promotes activation of the ER membrane-spanning kinase Ire1, which subsequently removes a translationally repressive cytoplasmically retained intron from the *HAC1* transcript through an atypical splicing event (Cox and Walter, 1996; Mori et al., 1996; Sidrauski et al., 1996). Spliced *HAC1* mRNA can be efficiently translated to produce a TF that activates a set of target genes, the most well-studied of which play clear roles in increasing ER volume, folding capacity, and quality control. Included in this set of canonical Hac1 targets are chaperones, such as BiP (*KAR2* in yeast), protein disulfide isomerase (*PDI1* in yeast), and lumenal Hsp70 (*LHS1*), as well as genes responsible for ER structure, lipid synthesis, and ER redox balance, such as thiol oxidase (*ERO1*; reviewed in Chapman et al., 1998).

An ORF microarray study identified ~400 mRNAs that were induced in response to UPR^{ER} activation in a Hac1-dependent manner, some of which were known to have clear function in ER biology, but many of which were not and whose function in the UPR^{ER} remains mysterious (Travers et al., 2000). Given that mRNA sequence levels can be misleading predictors of gene expression output, we hypothesized that some of the previously identified Hac1 transcriptional targets might actually be negatively regulated at the protein level via a LUTI-based mechanism. If this were true, it might help to explain why many of the genes that are transcriptionally induced by the UPR^{ER} do not result in protein misfolding in the ER when deleted and why—with few exceptions—roles in the UPR^{ER} remain undefined for most (Jonikas et al., 2009; Schuldiner and Weissman, 2013; Travers et al., 2000).

Through analysis of deep, parallel gene expression datasets, we found examples of previously defined Hac1 targets that display decreased protein production as a result of UPR^{ER} activation. We expanded our study beyond previously defined targets to identify 15 LUTI targets of Hac1. To enable robust detection of Hac1 targets, we developed a version of this TF that can be conditionally degraded. Using cells carrying this conditional allele, as well as wild-type (WT) and *hac1Δ* cells, we performed thorough profiling of gene expression: measuring mRNA, translation, and protein levels in response to UPR^{ER} activation, with or without Hac1. This allowed us to holistically define the Hac1-dependent cellular response to UPR^{ER} activation, which we found involves coordinated up- and downregulation of distinct protein groups. We observed, as expected, that protein synthesis and levels of ER proteins are increased upon UPR^{ER} activation. We also observed downregulation of ribosomal genes, as well as of genes involved in aerobic respiration. In the case of the latter group, observed protein expression decreases were partly controlled by Hac1-induced transcription of LUTI targets. Crippled aerobic respiration was found to provide a growth advantage to UPR^{ER}-induced cells, suggesting a cellular function for UPR^{ER}-mediated gene downregulation, and raising the possibility that a shift in cellular metabolism is a core part of the UPR^{ER}, at least in yeast. Our results suggest that LUTI-based regulation is a broadly used mechanism by which TFs coordinate up- and downregulation of target genes during cellular state changes.

RESULTS

Hac1 Induces Expression of LUTI Targets, Resulting in Protein Downregulation

To determine whether Hac1 induces LUTI-like repressive transcripts as part of the UPR^{ER}, we performed global gene expression measurements in WT and *hac1Δ* cells. We performed parallel mRNA sequencing (mRNA-seq) and ribosome profiling on untreated samples and those treated for 1 hr with either DTT or Tm to assay mRNA abundance and translation in response to UPR^{ER} activation (Figure 1B). We reasoned that canonical Hac1 targets should show a Hac1-dependent increase in both mRNA and translation with DTT or Tm treatment. In contrast, Hac1 LUTI targets may show an increase in mRNA, but regardless of mRNA-level changes should show a Hac1-dependent decrease in translation efficiency (TE) ([ribosome footprint RPKM])/([mRNA RPKM]) (RPKM = reads per kilobase per million mapped reads) with UPR^{ER} activation. The set of transcripts reported to be induced by Hac1 based on microarray analyses (Travers et al., 2000) were also generally induced at the mRNA level in our dataset, dependent on Hac1 (Figures 1C–1E). The most strongly upregulated transcripts included characterized UPR^{ER} targets *KAR2*, *ULI1*, *PDI1*, and *ERO1* (Figures 1C–1E; Chapman et al., 1998; Metzger and Michaelis, 2008). When we evaluated translation levels (based on ribosome footprint

Figure 1. Global Analysis of *HAC1*-Dependent Changes in Gene Expression during the UPR^{ER}

(A) Schematic of LUTI-mediated repression of gene expression.

(B) Harvesting scheme to compare mRNA and translation levels in wild-type (WT) and *hac1Δ* cells.

(C–E) Comparison of mRNA levels in cells with and without activation of an intact UPR^{ER}. Reported Hac1 targets were significantly (****$p < 0.0001$) more likely to be upregulated in a Hac1-dependent manner upon UPR^{ER} induction than the full gene set.

(F–H) Comparison of TEs for each gene with and without activation of an intact UPR^{ER}.

For (C) to (H), previously reported Hac1 targets (Travers et al., 2000) are shown as dark squares while all other genes are shown as light circles. See also Figure S1; Tables S1 and S2.

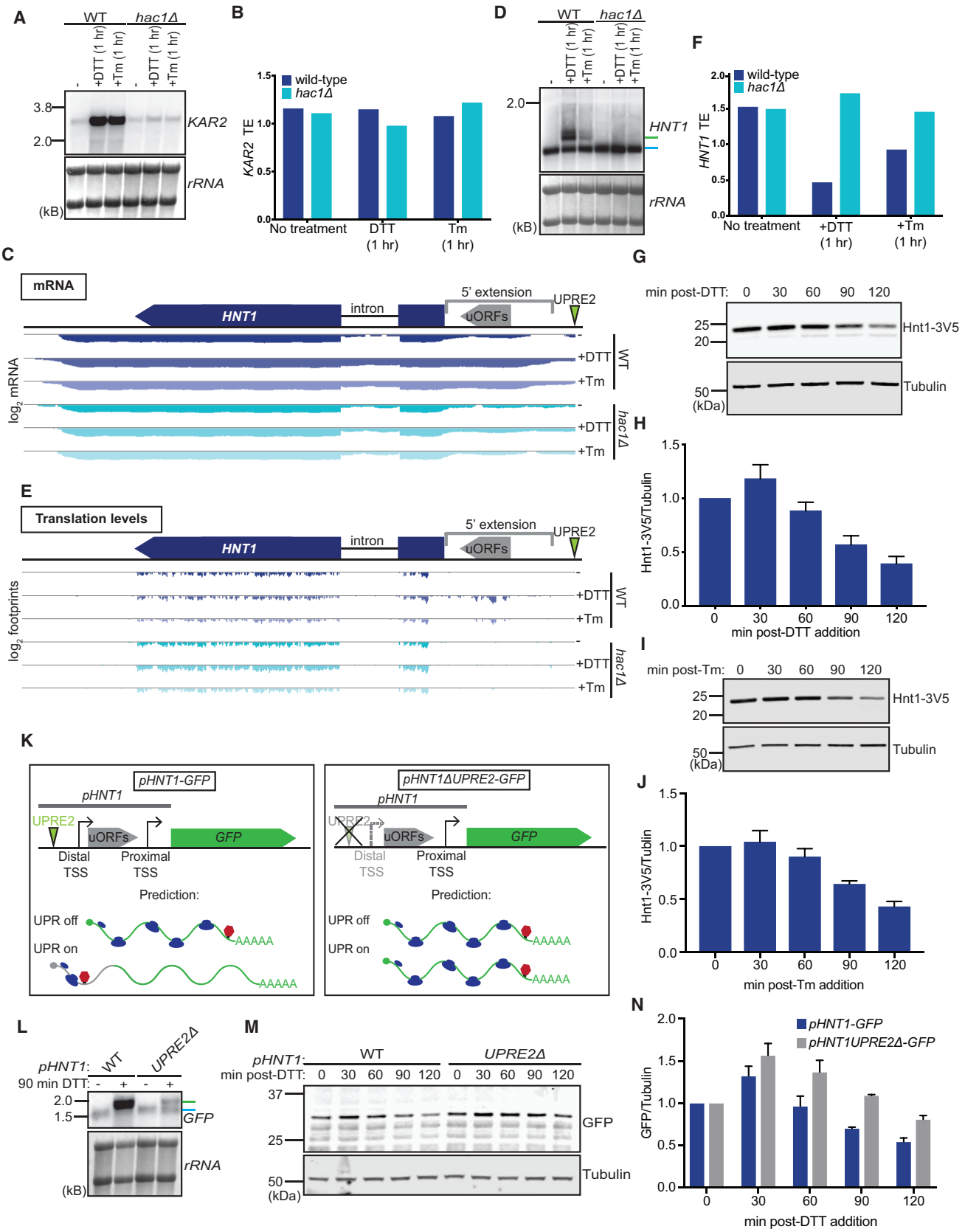

(legend on next page)

density), we saw prominent induction of the best-characterized Hac1 targets, as expected (Figures S1A–S1E). Overall, we identified 477 genes as showing a UPR^{ER}- and Hac1-dependent increase in translation of greater than 2-fold in this dataset. Genes in this group were strongly enriched for ER-localization and function, as expected (p value for ER = 2.64×10^{-14}; post-translational protein targeting to membrane, translocation = 1.33×10^{-6}; protein glycosylation = 1.58×10^{-5}; note that this set is based on analysis of DTT data, but Tm treatment yields similar results; Tables S1 and S2; Figures S1A–S1D).

Normalizing translation levels to mRNA levels allowed us to determine TEs across all annotated ORFs (Ingolia et al., 2009), enabling detection of Hac1-dependent TE shifts upon UPR^{ER} activation. Although UPR^{ER} activation has been reported to influence TEs of some genes (Krishnan et al., 2014; Labunskyy et al., 2014; Payne et al., 2008), little is known about the pervasiveness of or potential mechanisms behind such regulation. Rather, the UPR^{ER} has been defined primarily as a transcriptional response. Our data are consistent with this general model, with a clear cohort of UPR^{ER}-driven, Hac1-dependent upregulated transcripts seen (Figures 1C–1E). However, evidence for several dozen translationally regulated genes also emerged from our data. As expected, *HAC1* was one of the most strongly translationally upregulated genes upon DTT or Tm treatment (Figures 1F and 1G). An additional small subset of annotated Hac1 transcriptional targets seemed to show translational upregulation with UPR^{ER} activation, although the mechanistic basis for this remains unclear. The most prominent example was functionally uncharacterized ER-related gene *ULI1* (Metzger and Michaelis, 2008), which was also one of the most highly induced transcriptional targets of Hac1 (Figure 1E). The large increase in *ULI1* TE seen upon DTT treatment may point to a new translational mechanism linked to UPR^{ER} activation (Figures 1F–1H).

Additionally, several annotated Hac1 targets appeared to show a Hac1-dependent decrease in TE upon UPR^{ER} activation (Figures 1F–1H). This type of TF-dependent TE drop is a hallmark of LUTI-based regulation during meiotic differentiation (Cheng et al., 2018). Because transcription of poorly translated LUTI mRNAs decreases production of canonical well-translated transcript isoforms, TF-driven LUTI mRNA synthesis is detected in ribosome profiling datasets as translational repression (Cheng et al., 2018). We focused our attention on investigating *HNT1*, an annotated Hac1 target that consistently showed strong Hac1- and UPR^{ER}-dependent translational repression (Figures 1F–1H; Travers et al., 2000) by comparing its regulation with that of the most well-characterized Hac1 target, *KAR2*.

HNT1 is a conserved member of the histidine triad superfamily (Séraphin, 1992). Its cellular function remains unclear, although a mammalian family member has recently been implicated in regulation of m^7G mRNA caps, suggesting that this gene family may be involved in translation (Kiss et al., 2017a, 2017b). Before investigating *HNT1* regulation, we first confirmed that our dataset reported the expected mRNA induction of canonical UPR^{ER} targets. As expected, a single *KAR2* mRNA isoform accumulated in a UPR^{ER}- and Hac1-dependent manner, as judged by northern blotting (Figures 2A and S2A). *KAR2* mRNA was well-translated when present, with little change in TE seen upon UPR^{ER} activation (Figure 2B). In contrast, while UPR^{ER} activation resulted in increased overall *HNT1* mRNA levels (Figure S3B), it also resulted in a shift in the transcript isoforms present in cells. A longer *HNT1* mRNA species was observed by mRNA-seq and northern blotting following 1 hr of DTT or Tm treatment (Figures 2C, 2D, S2B, and S3C). The presence of the longer transcript was associated with lower TE values for the *HNT1* ORF and with translation of at least three uORFs in its extended 5′ leader (Figures 2E and 2F). Despite exhibiting hallmarks of LUTI-based regulation, the canonical *HNT1* transcript persisted after 1 hr of UPR^{ER} induction (Figures 2D, S2B, and S3C). Because the first LUTI case defined, $NDC80^{LUTI}$, resulted in complete disappearance of the canonical *NDC80* transcript when induced, we wondered whether the apparently weaker LUTI induction observed for *HNT1* during the UPR^{ER} would be sufficient to have an effect on Hnt1 protein levels. We epitope-tagged endogenous Hnt1 and performed western blotting to detect protein levels following UPR^{ER} induction. Within 2 hr of DTT or Tm treatment, Hnt1 levels dropped to less than 50% of their levels prior to drug treatment (Figures 2G–2J). We confirmed that, like canonical UPR^{ER} target *KAR2* (Figure S3A), production of the long *HNT1* transcript isoform was dependent on *IRE1*, and thus part of the canonical UPR^{ER} (Figure S3C).

We identified a strong type-2 UPR element (UPRE2), a DNA motif associated with Hac1 binding in the promoters of some UPR^{ER} targets (Patil et al., 2004), close to the distal *HNT1*

Figure 2. *HAC1*-Dependent Transcription of an Alternative Transcript Isoform Is Correlated with Decreased Protein Levels

(A) Northern blotting for *KAR2* shows the abundance of a single transcript isoform increases upon UPR^{ER} activation, dependent on *HAC1*.

(B) Comparison of *KAR2* TEs with and without UPR^{ER} activation.

(C) Annotation of *HNT1* mRNA expression during the UPR^{ER}. Upper: gene model. Lower: $\log_2$ mRNA (RPKM) showing an extension in transcript length upon UPR^{ER} activation in WT cells.

(D) Northern blotting for *HNT1* reveals an extended transcript isoform is produced upon UPR^{ER} activation, dependent on *HAC1*. Blue and green bars highlight canonical and extended transcripts, respectively.

(E) Annotation of *HNT1* translation during the UPR^{ER}. Upper: gene model. Lower: $\log_2$ footprints (RPKM) showing translation of uORFs in the extended transcript.

(F) Comparison of *HNT1* TEs with and without UPR^{ER} activation.

(G–J) A decrease in Hnt1-3V5 protein was observed upon UPR^{ER} activation with DTT (G and H) or Tm (I and J). Quantifications represent the average of three biological replicates with error bars representing SD.

(K) GFP reporters were constructed to assess the role of the UPRE2 in the *HNT1* distal promoter.

(L) Northern blotting for *GFP* shows that a longer transcript isoform is produced upon UPR^{ER} induction, but expression of the longer isoform is strongly reduced when the UPRE2 motif is disrupted. Blue and green bars highlight canonical and extended transcripts, respectively.

(M and N) A decrease in GFP protein was observed upon UPR^{ER} induction in cells harboring *pHNT1-GFP* but was less efficient in cells harboring *pHNT1ΔUPRE2-GFP*. Quantification represents the average of three biological replicates with error bars representing SD.

See also Figures S2 and S3.

Table 1. Hac1-Dependent LUTI Candidates

		Wild-type/*hac1Δ* Dataset		*AID-HAC1* Dataset		
Gene	Full Name	*HAC1*-Dependent Decrease in TE	*HAC1*-Dependent Extended Transcript	Hac1-Dependent Decrease in TE	Hac1-Dependent Extended Transcript	Monosome Shifted upon DTT Addition[a]
COX20	Cytochrome *c* OXidase	+	+	+	+	+
HNT1	Histidine triad NucleoTide-binding	+	+	+	+	+
MSK1	Mitochondrial aminoacyl-tRNA Synthetase, lysine (K)	+	+	+	+	–
SOM1	SOrting Mitochondrial	+	+	+	+	+
GTT1	GlutaThione Transferase	+	+	+	+	+
IRC4	Increased Recombination Centers	+	+	+	+	+
CRR1	CRH-Related	+	+	+	+	–
HEM1	HEMe biosynthesis	+	+	+	+	+
OXA1	cytochrome OXidase Activity	+	+	+[b]	+	+
NRG2	Negative Regulator of Glucose-controlled genes	+	+	+[b]	+	–
YPL067C	Histidine Triad with Channel	+	+	+	+	–
SRM1	Suppressor of Receptor Mutations	+	+	+	+	+
CTS1	ChiTinaSe	+	+	+[b]	+	–
PCM1	PhosphoaCetylglucosamine Mutase	+	+	+	+	+
YHB1	Yeast flavoHemogloBin	+	+	+	+	+
FLR1[c]	FLuconazole Resistance	+	+	–	+	–
PRY1[c]	Pathogen Related in Yeast	+	+[d]	+[b]	+[d]	–
SRL1[c]	Suppressor of Rad53 null Lethality	+	+	+[b]	+[d]	–
SET2[c]	SET domain-containing	+	+	–	+	–

Systematic analysis of mRNA-seq and TE data from WT and *hac1Δ* cells (Figure 1B) was used to predict LUTI candidates. Nineteen candidates were identified. Reanalysis of these same features using the *AID-HAC1* allele (Figure 4A) confirmed 15 of these candidates, and many were previously reported to show decreased translation upon Tm addition (Labunskyy et al., 2014).

[a]As reported in Payne et al. (2008).

[b]Hac1 dependence inconclusive.

[c]Called as LUTI candidates in WT/*hac1Δ* but not *AID-HAC1*.

[d]Difficult to definitively call for reasons including locus complexity.

TSS (Figure 2C). The location of the UPRE2, coupled with the observation that induction of the longer transcript was dependent on *HAC1*, led us to hypothesize that the long *HNT1* isoform was a direct Hac1 target. To test this hypothesis, we constructed reporters containing *GFP* under control of the extended promoter region of *HNT1*, with either an intact UPRE2 adjacent to the distal TSS or a mutated motif (Figure 2K). Following 90 min of DTT treatment, cells harboring *pHNT1-GFP* produced a high level of an extended *GFP* transcript isoform whose expression was severely reduced in the *pHNT1ΔUPRE2-GFP* mutant (Figures 2L, S2C, and S3D). GFP protein levels in the WT reporter, but not the UPRE2 mutant, mirrored those of Hnt1 following UPR^{ER} induction (Figures 2M and 2N). We concluded that *HNT1* is a LUTI target of Hac1 and that the UPR^{ER} involves coordinated activation and repression of target gene expression through Hac1-regulated alternative TSS usage. We suspected that *HNT1* might be just one of a class of "negative" targets of Hac1 and thus performed a systematic analysis of our data, searching for the expected signatures of Hac1 LUTI targets, including Hac1-dependent decreases in TE and appearances of 5′ extended transcripts (Cheng et al., 2018). We identified 18 additional potential LUTI targets (Table 1).

A Degradable Version of Hac1 Enables High-Confidence Identification of Its Targets

Confidently identifying Hac1-dependent targets of the UPR^{ER}, whether canonical (positive) or non-canonical (LUTI-based negative), was done here and previously by using comparison of WT cells with those deleted for *HAC1* or other core UPR^{ER} genes (Travers et al., 2000). While this has been a valuable approach, the risk in comparing gene expression measurements from WT cells and constitutive mutants is that it is difficult to ensure that secondary effects—on gene expression and in the form of genetic suppressors—are not confounding, resulting in misinterpretation of results. Such suppressors have been reported in *hac1Δ* cells, including in our strain background (Lee et al., 2003). We were concerned that perhaps our identification of non-canonical Hac1 targets might be an unexpected artifact of such secondary effects. We therefore replaced Hac1 with a version that contained an auxin-inducible degron (AID) tag and thus could be depleted on-demand by auxin addition. We found that *AID-HAC1* rescued the growth defect of *hac1Δ* cells grown with DTT, suggesting normal functionality (Figures 3A and 3B; Nishimura et al., 2009). AID-Hac1 was stable in the presence of auxin in strains lacking the exogenous plant *TIR1* F-box auxin receptor gene, but in strains carrying *TIR1*, AID-Hac1 that

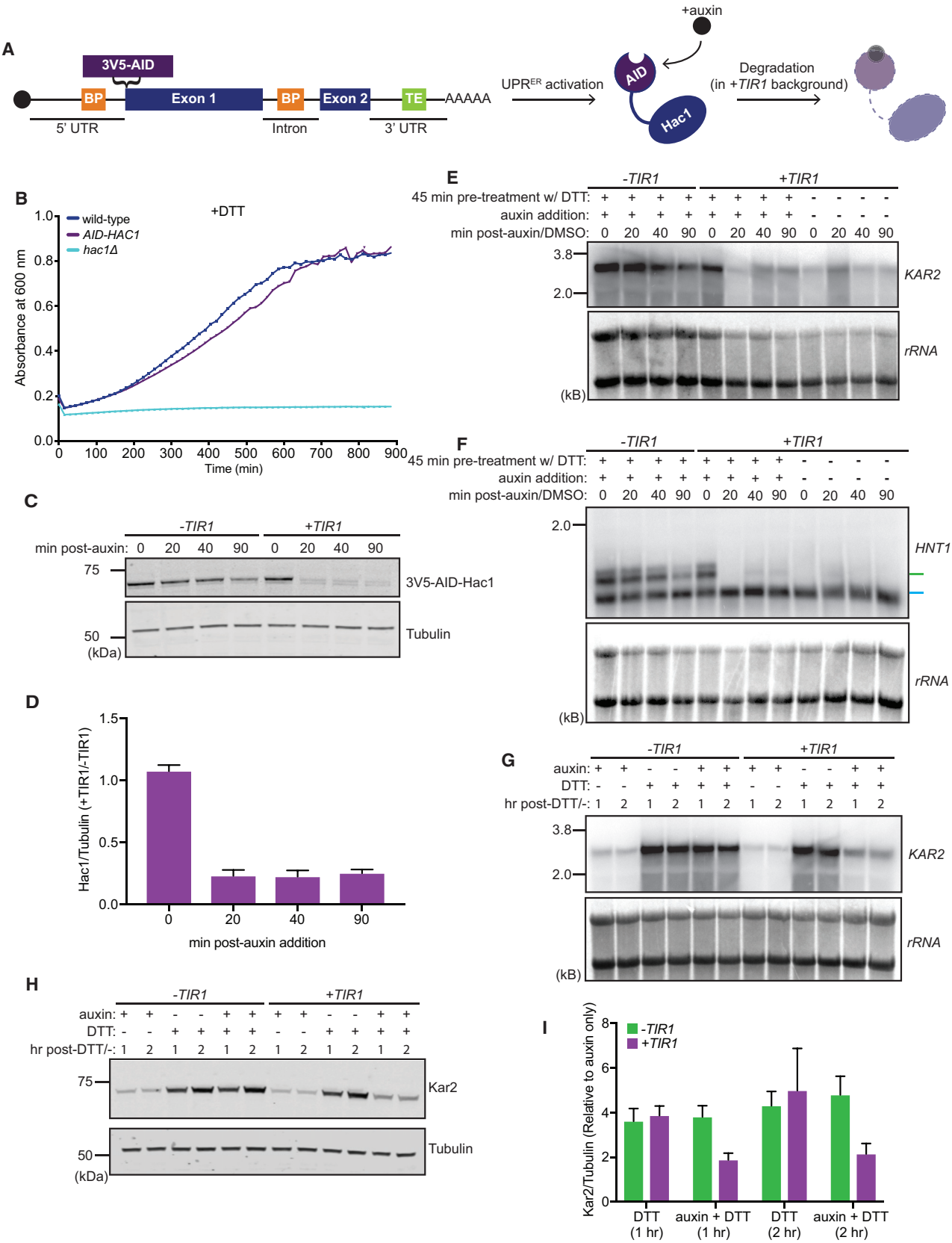

(legend on next page)

accumulated during DTT pre-treatment was rapidly depleted upon auxin addition (Figures 3C and 3D). Notably, AID-Hac1 protein was efficiently, but not fully, depleted in this background. As a result, we expected gene expression effects measured by comparing *AID-HAC1 TIR1* cells with and without auxin to be dampened relative to those from comparison of WT and *hac1Δ* cells.

Given that auxin-mediated degradation should be cytoplasmic, we were concerned that a persisting nuclear pool of AID-Hac1 may be capable of robustly carrying out its TF function, spatially isolated from the location of degradation. To investigate this, we analyzed expression of *KAR2* in cells that were treated with auxin following 45 min of DTT pre-treatment. *KAR2* levels were rapidly reduced under these conditions, suggesting that auxin-induced Hac1 degradation reduced its TF activity (Figures 3E and S2D). This result indicated that kinetic experiments using *AID-HAC1* cells might allow confident prediction of direct Hac1 transcriptional targets. The long isoform of *HNT1* (*HNT1*^{LUTI}) showed dynamics similar to that of the *KAR2* transcript, declining to undetectable levels within 20 min of auxin treatment following DTT pre-treatment (Figures 3F and S2E). This rapid timing provided additional evidence that *HNT1*^{LUTI} is a direct target of Hac1.

Although robust changes to transcription were observed by this strategy, effects on protein level of the canonical target Kar2 were not readily reversible upon auxin addition (data not shown), perhaps because Kar2 protein is not rapidly turned over under these circumstances. Because we have found assaying protein level to be useful in determining whether a given transcriptional target is positive or negative (Cheng et al., 2018), we reasoned that pre-treating cells with auxin and subsequently inducing the UPR^{ER} would be a more fruitful strategy. To this end, we pre-treated cells with auxin for 15 min and then added DTT for up to 2 hr. In cells lacking *TIR1*, *KAR2* mRNA and protein levels revealed the expected induction upon DTT treatment regardless of auxin addition (Figures 3G–3I and S2F). In contrast, in the *TIR1* background, DTT-dependent increases in *KAR2* transcript and protein levels were only observed if cells were pre-treated with vehicle. When pre-treated with auxin (depleting Hac1), efficient *KAR2* induction was largely prevented (Figures 3G–3I and S2F).

We next performed a new set of global gene expression measurements using the *AID-HAC1* strain background (Figure 4A). We again measured mRNA and translation levels, and additionally collected matched extract for mass spectrometry in order to more completely evaluate Hac1-dependent effects on cellular physiology during the UPR^{ER}. Global effects on mRNA and translation were similar to those observed in our previous WT/*hac1Δ* experiment (Figures 4B, 4C, and S4) but, as expected, were milder than observed when comparing WT and *hac1Δ* cells. Nevertheless, we observed UPR^{ER}- and Hac1-dependent activation of known Hac1 targets, including *KAR2*, *ERO1*, and *PDI1* (Figures 4B and S4). DTT-dependent induction of *HNT1*^{LUTI} was observed by mRNA-seq, but not in cells depleted of Hac1 (Figure 4D). As before, translation of *HNT1* was decreased in a UPR^{ER}- and Hac1-dependent manner and was associated with translation of uORFs in the extended 5′ leader unless cells were depleted of Hac1 (Figures 4C, 4E, 4F, and S4E–S4G). We confirmed the DTT and Hac1-dependent induction of *HNT1*^{LUTI}, as well as the correlated decrease in Hnt1 protein level, by northern and western blotting (Figures 4G–4I and S2G). We concluded that expression of *HNT1*^{LUTI} results in decreased Hnt1 protein levels, dependent on Hac1, suggesting that our original results were not an artifact of constitutive *HAC1* deletion (Figure 2).

Hac1 "Negative" Targets Include Genes Involved in ETC Function

We found that 15 of the original 19 annotated long transcript isoforms could be confirmed as UPR^{ER}- and Hac1-dependent in the *AID-HAC1* background (Table 1). Of the four that could not, two did not show the expected TE decrease and two showed the decrease independent of Hac1. These cases may be a result of yet undefined secondary effects in the delete background. We concluded that a set of LUTI targets is induced by Hac1 as part of the UPR^{ER}.

Several of the 15 Hac1-dependent LUTI-regulated genes were involved in electron transport chain (ETC) function, specifically in assembly of complex IV (cytochrome *c* oxidase), to which LUTI targets *COX20*, *OXA1*, and *SOM1* all contribute. We thus investigated the possibility that downregulation of ETC components might be linked to UPR^{ER} activation and partly controlled by LUTI-based regulation. We first examined the regulation of *COX20*, a gene responsible for Cox2 processing and subsequent assembly of complex IV (Hell et al., 2000). We confirmed the Hac1-dependent appearance of a dramatically 5′ extended transcript isoform upon UPR^{ER} activation by mRNA-seq (Figure 5A) and translation of a uORF near the 5′ end of this extended transcript, which was adjacent to a high-scoring UPRE2 (Figure S5B). Northern blotting for *COX20* revealed Hac1-dependent induction of a longer transcript upon DTT or Tm treatment, confirming that the mRNA-seq data did not simply reflect a partially overlapping transcript that excluded the *COX20* ORF (Figures

Figure 3. AID-Hac1 Is Functional, and Its Degradation Results in Observable Changes in the Levels of Hac1 Targets

(A) Schematic of the *AID-HAC1* allele. Regions of the 5′ UTR and intron that participate in base-pairing (BP) to repress translation were unperturbed, and the 3′ targeting element (TE) remained intact.

(B) *AID-HAC1* rescues the growth defect of *hac1Δ* in DTT.

(C and D) AID-Hac1 (anti-3V5) is efficiently degraded within 20 min of auxin addition following 45 min of DTT pre-treatment. Quantification represents the average of three biological replicates with error bars representing SD.

(E) Northern blotting for *KAR2* indicates that transcripts for canonical Hac1 targets decrease within 20 min of auxin addition following 45 min of DTT pre-treatment.

(F) Northern blotting for *HNT1* reveals that *HNT1*^{LUTI} behaves in the same manner as *KAR2* (see E) upon treatment with auxin following 45 min of DTT pre-treatment. Blue and green bars highlight canonical and extended transcripts, respectively.

(G) Pre-treating cells with auxin for 15 min prevents increased *KAR2* expression upon subsequent treatment with DTT.

(H and I) The effect of pre-treating cells with auxin for 15 min prior to DTT treatment manifests in observable changes in Kar2 protein levels. Quantification represents the average of three biological replicates with error bars representing SD.

See also Figure S2.

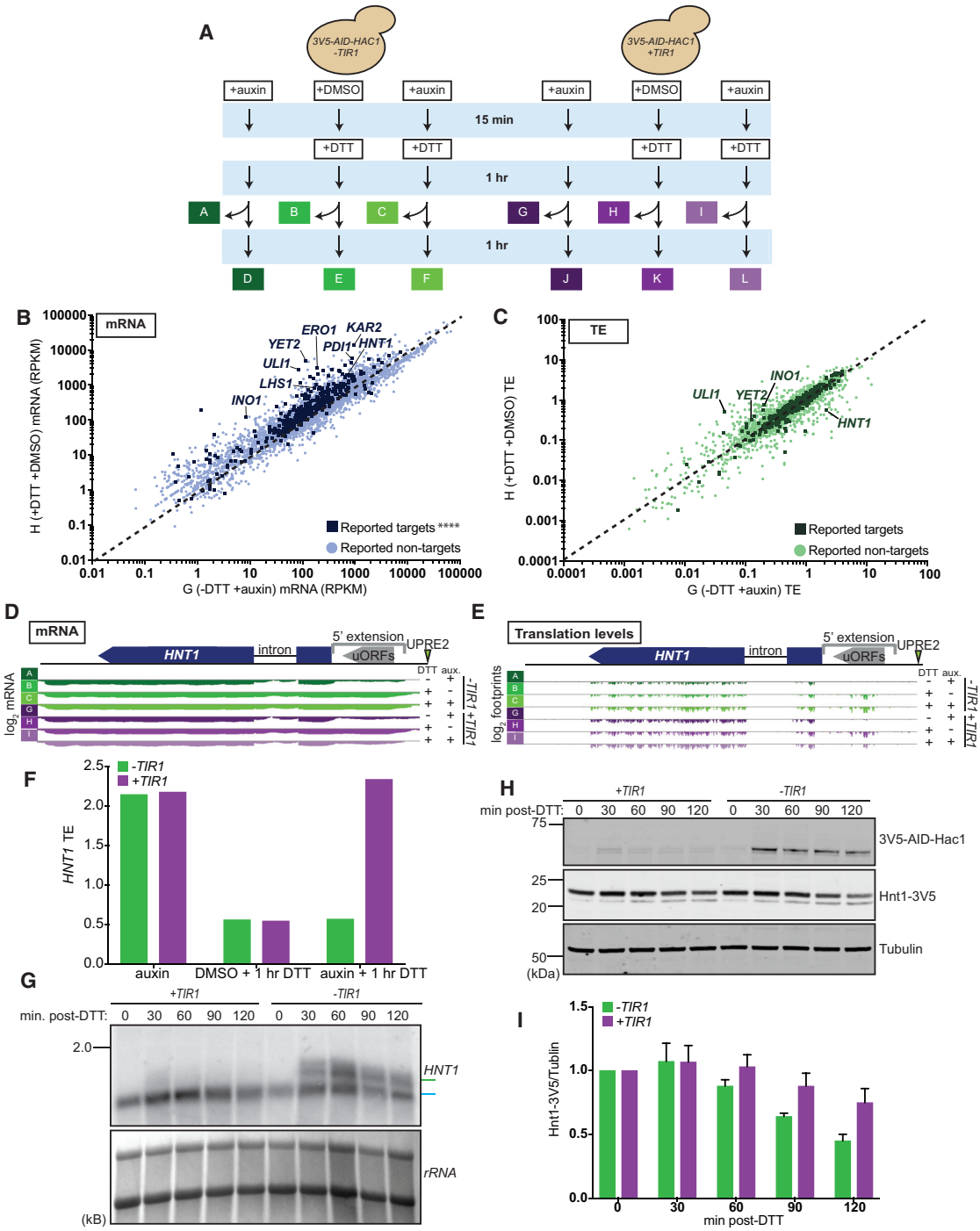

Figure 4. Global Analysis of UPR^{ER}-Dependent Changes in Gene Expression in the *AID-HAC1* Background

(A) Schematic of harvesting scheme.

(B) Comparison of mRNA levels in cells with and without DTT treatment in the *AID-HAC1* background. Reported Hac1 targets were significantly (****$p < 0.0001$) more likely to be upregulated upon UPR^{ER} induction than the full gene set.

(C) Comparison of TEs for each gene with and without DTT treatment in the *AID-HAC1* background. For panels (B) and (C), previously reported Hac1 targets (Travers et al., 2000) are shown as dark squares while all other genes are shown as light circles.

(D) Annotation of *HNT1* mRNA expression in the *AID-HAC1* background during the UPR^{ER}. Upper: gene model. Lower: $\log_2$ mRNA (RPKM) showing a Hac1-dependent *HNT1* transcript extension upon UPR^{ER} induction.

(E) Annotation of *HNT1* translation in the *AID-HAC1* background during the UPR^{ER}, as determined by the experiment described in (A). Upper: gene model. Lower: $\log_2$ footprints (RPKM) showing translation of uORFs in *HNT1*^{LUTI}.

(F) Comparison of *HNT1* TEs across samples (A) to (C) and (G) to (I).

(legend continued on next page)

5B, 5C, S2H, S2I, and S5A). This longer *COX20* transcript isoform was also dependent on *IRE1* (Figure S5D).

We were initially concerned that the bands representing the two *COX20* transcript isoforms did not show the stoichiometry expected based on our mRNA-seq data from either large-scale experiment, with the longer transcript reproducibly resulting in a much fainter band than the canonical transcript. We attribute this effect to the large size difference between the transcripts (0.8 kb versus approximately 2.6 kb; Figures 5A and S7K), as we observe that longer transcripts transfer less efficiently than shorter transcripts using our northern blotting protocol. Nevertheless, like the canonical UPR^{ER} target *KAR2*, production of $COX20^{LUTI}$ was abrogated with Hac1 depletion after 45 min of UPR^{ER} pre-activation, suggesting direct dependency on Hac1 (Figures 5B and S2H). Upon UPR^{ER} activation, we observed a decrease in *COX20* TE and Cox20-3V5 protein that was alleviated when Hac1 was depleted (Figures 5E, 5F, and S5C). This Cox20 protein decline was even more apparent in DTT-treated WT cells (Figures 5G and 5H), and was similar in extent but delayed in timing upon Tm treatment, consistent with the slower appearance of $COX20^{LUTI}$ upon Tm treatment (Figures 5C, 5I, 5J, S2I, and S5D). Importantly, levels of canonical target protein Kar2 continued to increase with Tm treatment over this time scale (Figure S5E). Also consistently, the *COX20* TE decreased more dramatically with DTT treatment than with Tm treatment (Figure 5D). We concluded that *COX20* is a LUTI target of Hac1, with protein levels that are downregulated as part of the UPR^{ER}.

UPR^{ER} Activation Drives a Global Proteomic and Metabolic Shift

Why do UPR^{ER}-activated cells couple upregulation of canonical targets, like *KAR2*, with downregulation of non-canonical ones, like *COX20*? In the case of *COX20*, the downregulation of its protein level was intriguing, given its role in ETC function. The UPR^{ER} in flies has been associated with induction of glycolytic enzymes and a cell-type specific metabolic shift to increased glycolytic flux (Lee et al., 2015). A similar shift from aerobic respiration to glycolysis is commonly observed in cancer cells and termed the ''Warburg effect'' in that context (Warburg, 1956). We sought to determine whether such an effect might be a core part of the Hac1-dependent UPR^{ER} by using additional global measurements in our *AID-HAC1* system. First, we performed metabolomic profiling, comparing cells with and without UPR^{ER} activation by Tm, and with and without Hac1 depletion. Of all glycolysis and tricarboxylic acid (TCA) intermediates measured, most did not change in a statistically significant manner in our experiment. Several did, however, and we noted that the two TCA intermediates (citrate and malate) that changed significantly between Hac1-containing and -depleted cells were lower in Tm-treated cells containing Hac1 than with its levels depleted, potentially suggesting reduced respiration in Hac1-containing UPR^{ER}-activated cells (Figure S6A). Glycolysis-associated metabolites tended to either remain roughly constant or be higher in UPR^{ER}-activated cells containing Hac1 (Figure S6A). These results were subtle and, while consistent with a shift from respiration in Hac1-containing UPR^{ER}-activated cells, did not provide definitive proof due to our inability to detect statistically significant shifts in many relevant intermediates with and without *TIR1*. We hypothesized that this may have resulted from the dampened range of effects that we note above in Hac1-depletion experiments compared with those using WT versus *hac1Δ* cells. Indeed, similar analyses in cells carrying *HAC1* showed consistent, significant disenrichment of TCA intermediates and enrichment of glycolytic intermediates with Tm treatment (Figure 6A).

To more comprehensively determine the degree to which UPR^{ER} activation may couple downregulation of specific physiological cellular processes, such as aerobic respiration, to upregulation of classic UPR^{ER} targets such as ER chaperones, we performed proteomic measurements in samples identical to those measured for mRNA and translation (Figures 4A–4C and S4). We used tandem mass tag (TMT)-based isobaric labeling to compare shifts in proteome composition with and without Hac1 depletion, and with and without UPR^{ER} activation. This experiment yielded a deep dataset, allowing comparison of the levels of 2,577 proteins with and without DTT and Hac1 (Figure 6B). The data were of high quality, revealing the expected patterns for Hnt1, Cox20, and canonical UPR^{ER} targets (Figure S6B). A broad view of the data revealed dramatic overall shifts in proteome composition with DTT addition, with a subset of these changes dependent on Hac1. A discrete cluster of 72 proteins, which included canonical targets Kar2, Ero1, Pdi1, and Lhs1, emerged as increased in a UPR^{ER}- and Hac1-dependent manner. Gene ontology (GO) analysis of the genes encoding these proteins (Figure 6B and Table S3) showed that they were strongly enriched for roles in protein transport and ER function. A second cluster of 197 proteins showed increased protein expression following UPR^{ER} activation that was delayed following Hac1 depletion. GO analysis of the genes encoding them revealed strong enrichment for proteolysis functions and the ER-associated degradation (ERAD) pathway (Figure 6B and Table S4; consistent with Travers et al., 2000). A third cluster of 282 proteins showed decreased protein levels with UPR^{ER} activation, with at least partial dependence on Hac1. The associated genes were heavily enriched for roles in translation and ribosome assembly (Figure 6B and Table S5). This observation is interesting, as the downregulation of translation is a well-defined aspect of the UPR^{ER} in higher eukaryotes (Walter and Ron, 2011). This effect has thus far been less clear in budding yeast studies, and our results suggest that it warrants revisiting. Most interestingly, given the Hac1-dependent LUTI regulation seen for Cox20 and our hypothesis that metabolism shifts away from respiration in UPR^{ER}-activated cells, the genes encoding the group of UPR^{ER}-dependent downregulated proteins was also enriched for roles in ATP synthesis coupled electron

(G) Northern blot analysis of $HNT1^{LUTI}$ mRNA expression with and without Hac1 degradation. Blue and green bars highlight canonical and extended transcripts, respectively.

(H and I) Western blot showing Hac1-dependent reduction in Hnt1-3V5 protein levels upon treatment with DTT (following 15 min of auxin pre-treatment). Quantification represents the average of three biological replicates with error bars representing SD.

See also Figures S2 and S4.

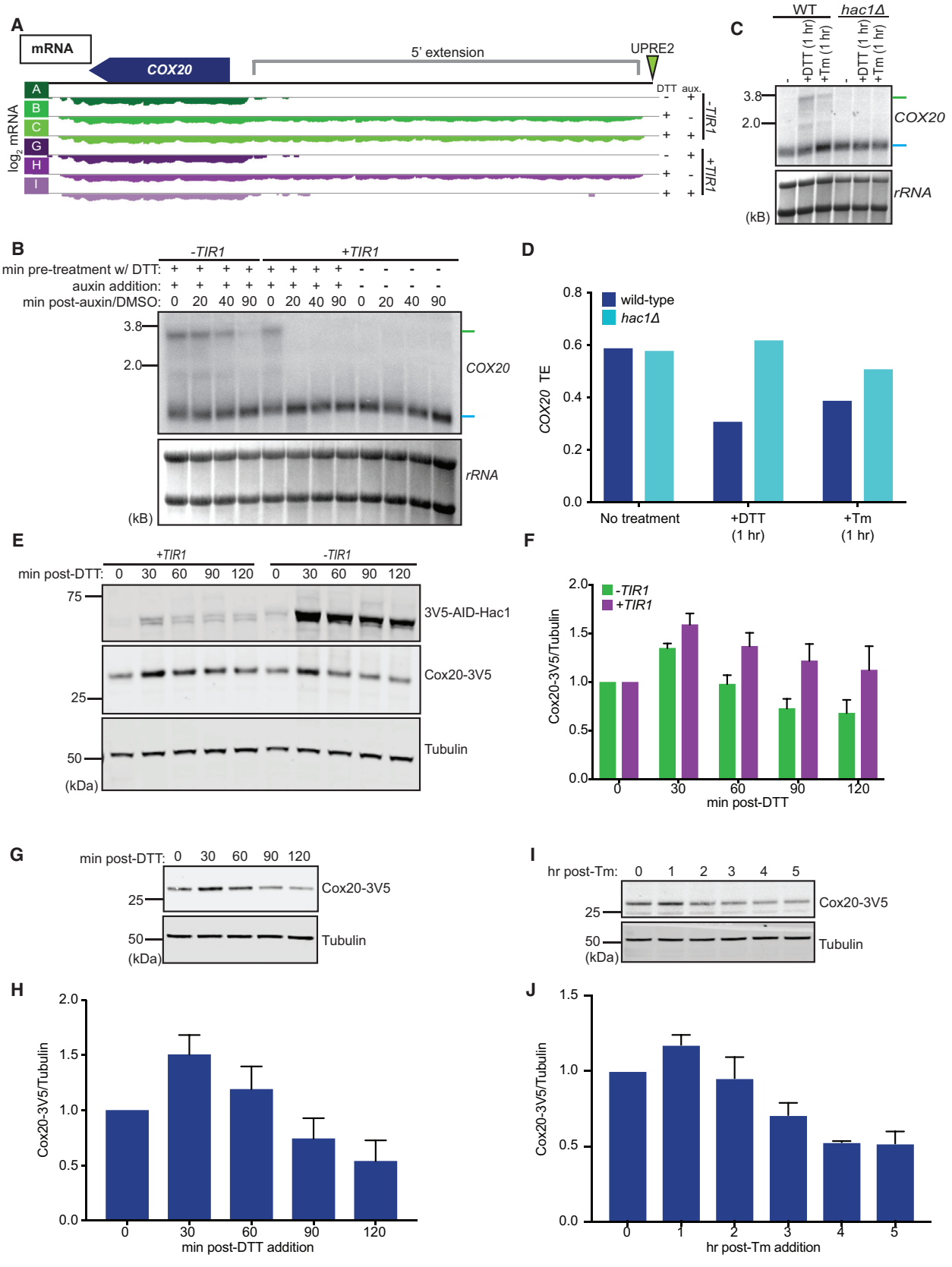

(legend on next page)

transport, oxidative phosphorylation, the ETC, cytochrome complexes, and the mitochondrial respiratory chain (Table S5). KEGG pathway analysis also revealed enrichment for components of the ETC and aerobic respiration ($p = 0.0027$) among these downregulated genes, further supporting a metabolic shift away from aerobic respiration as part of the UPR^{ER}. Finally, isolation of data for glycolytic enzymes revealed a complementary upregulation of protein levels that was dependent on UPR^{ER} activation, although only some of these increases were dependent on Hac1 (Figure S6C).

Because TMT-based measurements often yield values that appear dampened in range relative to other methods (Wenger et al., 2011), we also used label-free quantification (LFQ), an orthogonal approach, on the same samples. This allowed for better determination of the degree of specific protein level changes following UPR^{ER} activation. LFQ analysis revealed trends that mirrored those seen with TMT-based quantification, but that were less muted in degree (Figures S6B and S6D). As expected, UPR^{ER} induction still showed increased levels of canonical UPR^{ER} target proteins, such as Kar2 (Figure 6C). Untagged Hnt1 protein levels were dramatically reduced in a Hac1-dependent manner, to an even greater degree than observed for the epitope-tagged protein. The degree of Hnt1 decrease in Hac1-containing cells relative to cells depleted for Hac1 was roughly equivalent to the degree of Kar2 increase (Figure S6D), suggesting potential for a strong cellular effect from the Hac1-dependent induction of *HNT1^{LUTI}*. Cox20 showed a 2.4-fold decrease in UPR^{ER}-activated cells containing Hac1 compared with those depleted for it (Figure S6D), which was similar to the decrease observed for the epitope-tagged protein (Figures 5G–5J) and which suggests potential for a strong physiological effect.

Preventing Aerobic Respiration Ameliorates Cellular Growth Defects due to UPR^{ER} Activation

Oxygen consumption assays revealed a time-dependent, significant decrease in oxygen consumption rates (OCR) of cells treated with Tm (Figure 6D), consistent with a decrease in aerobic respiration in UPR^{ER}-activated cells. To investigate a potential functional role for downregulated aerobic respiration in the UPR^{ER}, we leveraged the fact that budding yeast cells can grow well in rich media in the absence of aerobic respiration resulting from mutation in ETC-related genes. We examined cells deleted for *PET100*, a gene that is required for assembly of ETC complex IV (Church et al., 1996). We compared cell doubling of untreated WT and *pet100Δ* cells in rich media, observing the expected moderate growth defect in the latter background (Figure 6E). We then repeated the experiment in the presence of DTT and observed that, while both WT and *pet100Δ* cells doubled more slowly than in untreated conditions, the previously observed growth defect in *pet100Δ* cells relative to WT was strongly suppressed (Figure 6F). In fact, under these conditions, *pet100Δ* cells robustly surpassed WT cells in their growth rate. Because of possible confounding effects of using a strong reducing agent like DTT for these experiments, we performed a similar analysis instead activating the UPR^{ER} by Tm addition, which is stable enough for use in plate-based growth assays, in contrast to DTT. Cell growth following dilution on plates containing 0–0.75 μg/mL Tm produced results similar to the DTT growth rate data (Figure 6G). WT cells formed larger colonies than *pet100Δ* cells without Tm, but with increasing Tm concentration, *pet100Δ* cells were able to surpass WT in growth ability. Based on these experiments, we concluded that downregulation of factors responsible for aerobic respiration, which accompanies UPR^{ER} activation and is partially modulated by Hac1 activity, is likely to be a functionally important component of the UPR^{ER} in yeast.

DISCUSSION

Here we report that, in addition to its characterized role in the induction of ER-related target genes during the UPR^{ER}, Hac1 also downregulates a set of genes by driving production of mRNAs that ultimately result in reduced protein levels. Hac1 thus coordinates up- and downregulation of distinct targets, contributing to a shift in the proteome and metabolism of UPR^{ER}-activated cells (Figure 6H). We report that Hac1-dependent transcription results in downregulation of at least 15 genes during the UPR^{ER} (Table 1). More broadly, our study provides a set of new examples of LUTI-based regulation, a recently defined mode of gene regulatory control that pervasively shapes the proteome of budding yeast cells during the meiotic program (Cheng et al., 2018; Tresenrider and Ünal, 2018). The fact that this regulation can be mediated by the conserved TF Hac1 as part of a conserved stress response suggests that it may be broadly used in transcriptional regulatory responses.

A key component of LUTI-based regulation is *cis*-silencing of the proximal TSS (Chia et al., 2017). While transcriptional interference is well-established (e.g., Cullen et al., 1984; Martens et al., 2004), LUTI-based regulation involves production of an interfering transcript containing a coding region that is translationally repressed. The ultimate effect of this regulation is

Figure 5. Cox20 Protein Levels Are Downregulated by a Hac1-Dependent LUTI Mechanism

(A) Annotation of *COX20* mRNA expression during the UPR^{ER}, as determined by the experiment described in Figure 4A. Upper: gene model. Lower: $\log_2$ mRNA (RPKM) showing an extension in *COX20* transcript length upon UPR^{ER} activation in cells not depleted of Hac1.

(B) Northern blotting for *COX20* confirms expression of an extended transcript isoform, which decreases within 20 min of auxin addition following 45 min of DTT pre-treatment. Blue and green bars highlight canonical and extended transcripts, respectively.

(C) The extended *COX20* transcript was also observed in WT cells upon treatment with DTT or Tm, but not *hac1Δ* cells. Blue and green bars highlight canonical and extended transcripts, respectively.

(D) Comparison of *COX20* TEs with and without UPR^{ER} activation.

(E and F) Western blot showing Hac1-dependent reduction in Cox20-3V5 protein levels upon treatment with DTT (following 15 min of auxin pre-treatment). Quantification represents the average of three biological replicates with error bars representing SD.

(G–J) A decrease in Cox20-3V5 protein in WT cells was observed by western blot upon UPR^{ER} activation with DTT (G and H) or Tm (I and J). Quantifications represent the average of three biological replicates with error bars representing SD.

See also Figures S2 and S5.

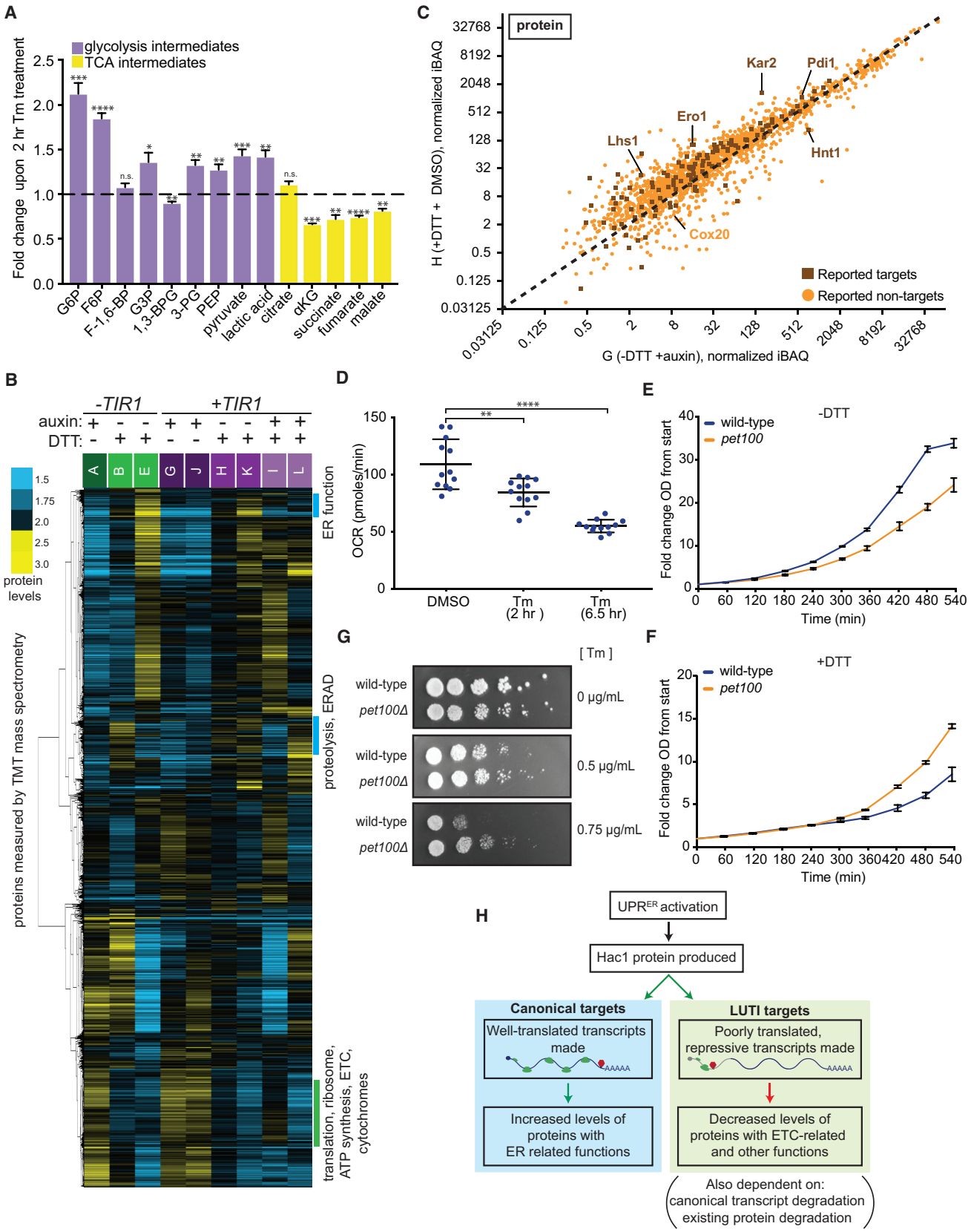

(legend on next page)

counterintuitive from a classical gene regulatory perspective, as it involves mRNA-inducing TFs acting effectively as repressors of gene expression and results in an uncoupling of overall mRNA and protein synthesis levels due to a greater importance of the isoform type than overall transcript levels in directing protein synthesis (Chen et al., 2017; Cheng et al., 2018). This can be seen in the Hac1 LUTI cases defined here, including *HNT1*, which was previously reported to be an upregulated UPR^{ER} target based on Hac1-dependent mRNA accumulation in response to UPR^{ER} activation (Travers et al., 2000). Consistently, we find that the total mRNA abundance for *HNT1* is increased during the UPR^{ER}, dependent on Hac1. However, expression of the Hac1-dependent LUTI transcript that accounts for this mRNA increase results in *decreased* protein production. Due to their relative ease of measurement, mRNA abundance values have been widely used as a proxy for gene expression output. While these measurements are undoubtedly useful and may accurately predict protein level changes in many instances, they can also be misleading. *HNT1* is a prime example of this in the simple and well-defined cellular response explored here. It is likely that many other existing gene expression datasets hold such examples, which may lead to misinterpretation of the cellular consequences of transcriptional responses.

While cases like *HNT1* are particularly striking, an overall mRNA increase is not necessarily seen in cases of LUTI production. Most of the new cases identified here instead exhibit a shift in the type of mRNA made without dramatically altering total mRNA quantity for a given gene. In these cases, mRNA levels are uninformative unless this information is integrated with translation data, and ideally measurements of protein, the ultimate gene expression output. Our use of integrated measurements from matched extract enabled a view of the UPR^{ER} gene expression program that would have been impossible to gain from analysis of existing gene expression datasets. For example, matched protein measurements in our study were key to showing that this unconventional mechanism has a cellular effect. Our protein data, which shows decreases in levels of LUTI-regulated proteins within 1–2 hr of UPR^{ER} activation, argue that active degradation of existing protein pools is likely also occurring under our experimental conditions, although we do not yet know the mechanism for the proteins explored here. Similarly, for this mechanism to be effective, transcript half-lives must be relatively short. While transcript destabilization is actively achieved during periods of UPR^{ER} activation for a subset of ER-localized mRNAs by regulated Ire1-dependent decay in some organisms (Hollien et al., 2009; reviewed in Maurel et al., 2014), this mechanism has not been observed in budding yeast. A recent study, however, reports mRNA half-lives in budding yeast to be much shorter than previously thought (Chan et al., 2017), suggesting that an additional mechanism for degradation of canonical transcripts of LUTI-regulated genes may not be required for this regulation to be rapid and effective.

Our study is not the first to suggest that the UPR^{ER} may directly or indirectly result in translational downregulation of a set of genes. Several studies have investigated this possibility and reanalysis of their data, in light of our LUTI model and complementary measurements, reveals results consistent with our findings. For example, microarray analyses of polysome fractions with and without DTT treatment showed that ribosome biogenesis genes were translationally repressed in a DTT-dependent manner, while canonical targets, such as *ERO1*, were well translated under these conditions (Payne et al., 2008). Interestingly, 10 of the 15 Hac1 LUTI targets that we annotate here—including *HNT1* and *COX20*—were among the genes detected in that study to show a DTT-dependent shift from polysomes to a sub-polysome fraction, indicating translational repression (Table 1). More recently, mRNA-seq and ribosome profiling was reported from cells with and without Tm treatment (Labunskyy et al., 2014). This study concluded that genes that were upregulated in response to Tm-driven UPR^{ER} activation tended to be transcriptional targets of Hac1 and that downregulated targets tended to be regulated at the level of TE (Labunskyy et al., 2014). This is consistent with our finding that Hac1 acts as a transcriptional activator for canonical targets and indirectly acts as a translational repressor for LUTI targets. Intriguingly, the Tm-dependent translationally downregulated genes in this previous ribosome profiling study were enriched for roles in ATP metabolic processes ($p = 0.026$) and mitochondria ($p = 0.030$), and several ETC-related genes were in this set, including two that are required for complex IV assembly (Table S6; Labunskyy et al., 2014). Although their results are consistent with our data, neither of these previous studies included strains deleted or depleted for *HAC1*, so the degree to which effects were dependent on Hac1 was unclear, and the lack of transcript isoform data available precludes reanalysis for other features of LUTI-based regulation.

Our study reveals two separate but linked key findings: the existence of Hac1-dependent LUTI-based regulation and

Figure 6. Induction of the UPR^{ER} Results in Coordinated Up- and Downregulation of Distinct Protein Classes and Promotes a Metabolic Shift

(A) Metabolite levels following Tm treatment of WT cells. Average fold change of six technical replicates is shown, with error bars representing SEM. A t test was used to evaluate significance. *$p < 0.05$, **$p < 0.01$, ***$p < 0.001$, ****$p < 0.0001$.

(B) Proteins quantified by TMT-based mass spectrometry are clustered by abundance patterns, with each normalized to the same total protein level across the row to enable comparison of trends. Proteins involved in ER function, proteolysis, and ERAD appear to be upregulated in a Hac1-dependent manner (blue bars). Proteins involved in translation, ribosome biogenesis, ATP synthesis, the ETC, and cytochromes appear to be downregulated in a Hac1-dependent manner (green bar).

(C) Protein levels obtained via label-free mass spectrometry analysis are plotted with previously reported Hac1 transcriptional targets shown as dark squares.

(D) Basal OCRs were measured following treatment of WT cells with Tm. Rates from replicate wells are plotted, with overlaid bars representing average and SD. Rates were adjusted to normalize for optical density (OD) differences. A Mann-Whitney test was used to statistically compare OCR. **$p < 0.01$, ****$p < 0.0001$.

(E and F) Growth of WT and *pet100Δ* cells with and without DTT. Average fold change in OD relative to the starting OD for three biological replicates is plotted against time, with error bars representing SD.

(G) Serial dilution-based growth assay of WT and *pet100Δ* cells on plates containing 0–0.75 μg/mL Tm.

(H) Model for Hac1-coordinated up- and downregulation during the UPR^{ER}.

See also Figure S6 and Tables S3, S4, S5, and S6.

coordinated up- and downshifting of levels of distinct protein groups during the UPR^{ER}. We propose, based on examples such as *COX20*, that the downregulation of genes involved in aerobic respiration observed during the UPR^{ER} is at least partially mediated by Hac1-based induction of repressive mRNA isoforms. However, we do not find evidence that all respiratory protein downregulation is dependent on this mechanism. For most of the ETC proteins that we measured to be reduced during UPR^{ER} activation, no associated alternative transcript isoforms were observed. This could be a result of the challenges in predicting alternative transcript isoforms based on mRNA-seq data alone, as we did in this study as a necessity, but it seems unlikely that LUTI-based regulation can directly explain the downregulation of all proteins observed here to decrease during the UPR^{ER}. It is more likely that either a few LUTI-regulated genes act as linchpin components that cause remaining complex members to become unstable or that there are parallel, potentially synergistic mechanisms to decrease levels of respiratory proteins during the UPR^{ER}. The cellular consequence of our newly identified cases of Hac1-dependent, LUTI-based gene repression is another outstanding question. We note an apparent enrichment for ETC function among the group, but have not identified enough cases to confidently assay statistical significance for LUTI-based regulation for this or other processes. It is likely, however, that ETC regulation is not the function of all newly proposed Hac1 LUTI mRNAs. Although several of the 15 genes encode mitochondrial proteins, most do not. Additionally, some of these genes, including *HNT1*, have such poorly defined cellular roles that determining the possible importance of their downregulation during the UPR^{ER} is difficult at this time.

Our proteomic data suggest a reallocation of cellular resources in UPR^{ER}-activated cells from ribosome biogenesis to ER function, and away from respiration. It is not surprising that a stress response would require a shift in proteome content, but in this case it is unclear why the Warburg-like shift in ATP-generation mode would bolster cellular fitness during the UPR^{ER} (Figure 6; Lee et al., 2015). Nonetheless, our results show that such a shift occurs and is advantageous, as cells without the ability to respire show a growth advantage relative to WT cells when grown in UPR^{ER}-activating conditions. While this result suggests that this shift is a relevant functional component of the UPR^{ER}, it does not explain *why* this is the case. It has been proposed that reduction of TCA cycle activity associated with the Warburg effect seen in cancer cells allows acetyl-coenzyme A to be shunted toward the robust new lipid synthesis required for membrane expansion that accompanies rapid cell division (Vander Heiden et al., 2009). A similar explanation is enticing in this case, as one of the hallmarks of UPR^{ER} activation is an increase in ER membrane volume, which requires new lipid synthesis and membrane expansion. It is alternatively possible that it is important to downregulate an alternative ETC function for the UPR^{ER}. For example, it has recently been shown that the redox function of the ETC through NAD^+ recycling is responsible for the growth defect seen in ETC-deficient mammalian cells (Titov et al., 2016).

Why do UPR^{ER}-activated cells employ the LUTI mechanism for downregulation of a subset of targets? In principle, a transcriptional repressor that is linked to UPR^{ER} activation should allow a similar overall effect, although to our knowledge no such regulator has been identified. We argue, however, that LUTI-based regulation is as effective as this alternative classical mode of regulation. We note that several Hac1-dependent LUTI target proteins, including Cox20 and Som1, show robust *upregulation* in response to DTT in the absence of Hac1. Hac1-dependent induction of the LUTI transcript in these cases appears effective at preventing and even reversing these protein level increases. Furthermore, this modular mechanism of regulation allows cells to use pre-existing *trans* factors for both up- and downregulation of targets, precluding the need for an additional protein to act as a dedicated transcriptional repressor (Chen et al., 2017; Cheng et al., 2018). Perhaps most importantly, a major advantage of this mechanism is that the use of a single TF—Hac1 in this case—allows for direct coordination of upregulation of some genes with downregulation of others (Cheng et al., 2018). This type of coordination is an attractive strategy for mediating rapid cellular responses to acute stress. The fact that a well-studied, conserved stress response program employs this unconventional mode of gene regulation suggests that LUTI-based regulation may be broadly used to modulate gene expression in contexts of cellular state change. Construction of new, integrated datasets aimed at identifying such regulation, along with revisiting traditional conceptual models of gene expression, will be required to ultimately determine whether this is the case.

STAR★METHODS

Detailed methods are provided in the online version of this paper and include the following:

- KEY RESOURCES TABLE
- CONTACT FOR REAGENT AND RESOURCE SHARING
- EXPERIMENTAL MODEL AND SUBJECT DETAILS
  - Yeast Strain Construction
  - Yeast Growth Conditions
- METHOD DETAILS
  - Sample Collection for Sequencing Experiments
  - Additional Sample Collection for Protein/RNA
  - Growth Curves
  - Plate-Based Growth Assays
  - Northern Blotting
  - Western Blotting
  - Ribosome Profiling Library Generation
  - mRNA-Sequencing Library Generation
  - Sequencing
  - Metabolomic Profiling
  - Oxygen Consumption Assay
  - Mass Spectrometry
- QUANTIFICATION AND STATISTICAL ANALYSES
  - Sequence Alignments and Analysis
  - LUTI Identification
  - Translation Efficiency Calculations
  - Statistical Analyses
  - Western Blot Quantification
  - Analysis of TMT Mass Spectrometry
  - Analysis of LFQ Mass Spectrometry
- DATA AND SOFTWARE AVAILABILITY

SUPPLEMENTAL INFORMATION

Supplemental Information includes seven figures and seven tables and can be found with this article online at https://doi.org/10.1016/j.devcel.2018.06.016.

ACKNOWLEDGMENTS

Thanks to Jonathan Weissman, James Olzmann, Elçin Ünal, and Andy Dillin for helpful comments on the manuscript. Thanks to Erica Moehle and the Dillin lab for use of and assistance with their Seahorse XF analyzer, and to members of the Brar and Ünal labs, Christopher Mugler, and Leon Chan for experimental suggestions. We thank Mark Rose for the generous gift of the Kar2 antibody to the Br-Ün lab. This work was funded by the NIH (DP2-GM-119138), investigator awards from the Alfred P. Sloan Foundation and Pew Charitable Trusts, and UC-Berkeley start-up funding to G.A.B. D.K.N. and C.A.B. are funded by NIH/NCI grant R01CA172667. M.J., S.H., and A.K. are funded by Columbia start-up funding. K.M.V.D. and A.H. were funded by NSF pre-doctoral fellowships (DGE1106400 and DGE1752814, respectively). K.M.V.D., A.H., and G.M.O. were also funded by NIH training grants to the MCB department (T32 GM 0007232 and T32 HG 00047).

AUTHOR CONTRIBUTIONS

K.M.V.D. and G.A.B. conceived the study. Sequencing experiments were performed by K.M.V.D. and G.A.B. Protein mass spectrometry was performed by S.H., A.K., and M.J. Metabolite analyses were performed by C.A.B. All other experiments were performed by K.M.V.D. with assistance from T.C. and G.M.O. Data analysis was performed by K.M.V.D., C.A.B., D.K.N., M.J., A.H., and G.A.B. K.M.V.D. and G.A.B. wrote and edited the manuscript.

DECLARATION OF INTERESTS

All authors declare no competing interests.

Received: February 11, 2018
Revised: May 16, 2018
Accepted: June 20, 2018
Published: July 16, 2018

REFERENCES

Aragón, T., van Anken, E., Pincus, D., Serafimova, I.M., Korennykh, A.V., Rubio, C.A., and Walter, P. (2009). Messenger RNA targeting to endoplasmic reticulum stress signalling sites. Nature *457*, 736–740.

Bowring, C.E., and Llewellyn, D.H. (2001). Differences in HAC1 mRNA processing and translation between yeast and mammalian cells indicate divergence of the eukaryotic ER stress response. Biochem. Biophys. Res. Commun. *287*, 789–800.

Brar, G.A., Yassour, M., Friedman, N., Regev, A., Ingolia, N.T., and Weissman, J.S. (2012). High-resolution view of the yeast meiotic program revealed by ribosome profiling. Science *335*, 552–557.

Chan, L.Y., Mugler, C.F., Heinrich, S., Vallotton, P., and Weis, K. (2017). Non-invasive measurement of mRNA decay reveals translation initiation as the major determinant of mRNA stability. bioRxiv. https://doi.org/10.1101/214775.

Chapman, R., Sidrauski, C., and Walter, P. (1998). Intracellular signaling from the endoplasmic reticulum to the nucleus. Annu. Rev. Cell Dev. Biol. *14*, 459–485.

Chen, J., Tresenrider, A., Chia, M., McSwiggen, D.T., Spedale, G., Jorgensen, V., Liao, H., van Werven, F.J., and Ünal, E. (2017). Kinetochore inactivation by expression of a repressive mRNA. Elife *6*, https://doi.org/10.7554/eLife.27417.

Cheng, Z., Otto, G.M., Powers, E.N., Keskin, A., Mertins, P., Carr, S., Jovanovic, M., and Brar, G.A. (2018). Pervasive, coordinated protein level changes driven by transcript isoform switching during meiosis. Cell *172*, 910–923.

Chia, M., Tresenrider, A., Chen, J., Spedale, G., Jorgensen, V., Ünal, E., and van Werven, F.J. (2017). Transcription of a 5′ extended mRNA isoform directs dynamic chromatin changes and interference of a downstream promoter. Elife *6*, https://doi.org/10.7554/eLife.27420.

Church, C., Chapon, C., and Poyton, R.O. (1996). Cloning and characterization of PET100, a gene required for the assembly of yeast cytochrome c oxidase. J. Biol. Chem. *271*, 18499–18507.

Cox, J., and Mann, M. (2008). MaxQuant enables high peptide identification rates, individualized p.p.b.-range mass accuracies and proteome-wide protein quantification. Nat. Biotechnol. *26*, 1367–1372.

Cox, J.S., and Walter, P. (1996). A novel mechanism for regulating activity of a transcription factor that controls the unfolded protein response. Cell *87*, 391–404.

Cullen, B.R., Lomedico, P.T., and Ju, G. (1984). Transcriptional interference in avian retroviruses—implications for the promoter insertion model of leukaemogenesis. Nature *307*, 241–245.

Haghighat, A., Svitkin, Y., Novoa, I., Kuechler, E., Skern, T., and Sonenberg, N. (1996). The eIF4G-eIF4E complex is the target for direct cleavage by the rhinovirus 2A proteinase. J. Virol. *70*, 8444–8450.

Han, J., and Kaufman, R.J. (2017). Physiological/pathological ramifications of transcription factors in the unfolded protein response. Genes Dev. *31*, 1417–1438.

Hell, K., Tzagoloff, A., Neupert, W., and Stuart, R.A. (2000). Identification of Cox20p, a novel protein involved in the maturation and assembly of cytochrome oxidase subunit 2. J. Biol. Chem. *275*, 4571–4578.

Hinnebusch, A.G. (1993). Gene-specific translational control of the yeast GCN4 gene by phosphorylation of eukaryotic initiation factor 2. Mol. Microbiol. *10*, 215–223.

Hollien, J., Lin, J.H., Li, H., Stevens, N., Walter, P., and Weissman, J.S. (2009). Regulated Ire1-dependent decay of messenger RNAs in mammalian cells. J. Cell Biol. *186*, 323–331.

Homann, O.R., and Johnson, A.D. (2010). MochiView: versatile software for genome browsing and DNA motif analysis. BMC Biol. *8*, 49.

De Hoon, M.J.L., Imoto, S., Nolan, J., and Miyano, S. (2004). Open source clustering software. Bioinforma. Oxf. Engl. *20*, 1453–1454.

Ingolia, N.T., Ghaemmaghami, S., Newman, J.R.S., and Weissman, J.S. (2009). Genome-wide analysis in vivo of translation with nucleotide resolution using ribosome profiling. Science *324*, 218–223.

Jonikas, M.C., Collins, S.R., Denic, V., Oh, E., Quan, E.M., Schmid, V., Weibezahn, J., Schwappach, B., Walter, P., Weissman, J.S., et al. (2009). Comprehensive characterization of genes required for protein folding in the endoplasmic reticulum. Science *323*, 1693–1697.

Keshishian, H., Burgess, M.W., Gillette, M.A., Mertins, P., Clauser, K.R., Mani, D.R., Kuhn, E.W., Farrell, L.A., Gerszten, R.E., and Carr, S.A. (2015). Multiplexed, quantitative workflow for sensitive biomarker discovery in plasma yields novel candidates for early myocardial injury. Mol. Cell. Proteomics *14*, 2375–2393.

Kiss, D.L., Waters, C.E., Ouda, I.M., Saldivar, J.C., Karras, J.R., Amin, Z.A., Mahrous, S., Druck, T., Bundschuh, R.A., Schoenberg, D.R., et al. (2017a). Identification of Fhit as a post-transcriptional effector of Thymidine Kinase 1 expression. Biochim. Biophys. Acta *1860*, 374–382.

Kiss, D.L., Baez, W., Huebner, K., Bundschuh, R., and Schoenberg, D.R. (2017b). Impact of FHIT loss on the translation of cancer-associated mRNAs. Mol. Cancer *16*, 179.

Krishnan, K., Ren, Z., Losada, L., Nierman, W.C., Lu, L.J., and Askew, D.S. (2014). Polysome profiling reveals broad translatome remodeling during endoplasmic reticulum (ER) stress in the pathogenic fungus *Aspergillus fumigatus*. BMC Genomics *15*, 159.

Labunskyy, V.M., Gerashchenko, M.V., Delaney, J.R., Kaya, A., Kennedy, B.K., Kaeberlein, M., and Gladyshev, V.N. (2014). Lifespan extension conferred by endoplasmic reticulum secretory pathway deficiency requires induction of the unfolded protein response. PLoS Genet. *10*, e1004019.

Langmead, B., and Salzberg, S.L. (2012). Fast gapped-read alignment with Bowtie 2. Nat. Methods *9*, 357–359.

Law, G.L., Bickel, K.S., MacKay, V.L., and Morris, D.R. (2005). The undertranslated transcriptome reveals widespread translational silencing by alternative 5′ transcript leaders. Genome Biol. *6*, R111.

Lee, J.E., Oney, M., Frizzell, K., Phadnis, N., and Hollien, J. (2015). *Drosophila melanogaster* activating transcription factor 4 regulates glycolysis during endoplasmic reticulum stress. G3 (Bethesda) *5*, 667–675.

Lee, K., Neigeborn, L., and Kaufman, R.J. (2003). The unfolded protein response is required for haploid tolerance in yeast. J. Biol. Chem. *278*, 11818–11827.

Longtine, M.S., McKenzie, A., Demarini, D.J., Shah, N.G., Wach, A., Brachat, A., Philippsen, P., and Pringle, J.R. (1998). Additional modules for versatile and economical PCR-based gene deletion and modification in *Saccharomyces cerevisiae*. Yeast *14*, 953–961.

Louie, S.M., Grossman, E.A., Crawford, L.A., Ding, L., Camarda, R., Huffman, T.R., Miyamoto, D.K., Goga, A., Weerapana, E., and Nomura, D.K. (2016). GSTP1 is a driver of triple-negative breast cancer cell metabolism and pathogenicity. Cell Chem. Biol. *23*, 567–578.

Martens, J.A., Laprade, L., and Winston, F. (2004). Intergenic transcription is required to repress the *Saccharomyces cerevisiae* SER3 gene. Nature *429*, 571–574.

Maurel, M., Chevet, E., Tavernier, J., and Gerlo, S. (2014). Getting RIDD of RNA: IRE1 in cell fate regulation. Trends Biochem. Sci. *39*, 245–254.

Metzger, M.B., and Michaelis, S. (2008). Analysis of quality control substrates in distinct cellular compartments reveals a unique role for Rpn4p in tolerating misfolded membrane proteins. Mol. Biol. Cell *20*, 1006–1019.

Mori, K., Kawahara, T., Yoshida, H., Yanagi, H., and Yura, T. (1996). Signalling from endoplasmic reticulum to nucleus: transcription factor with a basic-leucine zipper motif is required for the unfolded protein-response pathway. Genes Cells *1*, 803–817.

Moseley, J.L., Page, M.D., Alder, N.P., Eriksson, M., Quinn, J., Soto, F., Theg, S.M., Hippler, M., and Merchant, S. (2002). Reciprocal expression of two candidate Di-iron enzymes affecting photosystem i and light-harvesting complex accumulation. Plant Cell *14*, 673–688.

Nishimura, K., Fukagawa, T., Takisawa, H., Kakimoto, T., and Kanemaki, M. (2009). An auxin-based degron system for the rapid depletion of proteins in nonplant cells. Nat. Methods *6*, 917–922.

Ogawa, N., and Mori, K. (2004). Autoregulation of the HAC1 gene is required for sustained activation of the yeast unfolded protein response. Genes Cells *9*, 95–104.

Otto, G.M., and Brar, G.A. (2018). Seq-ing answers: uncovering the unexpected in global gene regulation. Curr. Genet. https://doi.org/10.1007/s00294-018-0839-3.

Patil, C.K., Li, H., and Walter, P. (2004). Gcn4p and novel upstream activating sequences regulate targets of the unfolded protein response. PLoS Biol. *2*, E246.

Payne, T., Hanfrey, C., Bishop, A.L., Michael, A.J., Avery, S.V., and Archer, D.B. (2008). Transcript-specific translational regulation in the unfolded protein response of *Saccharomyces cerevisiae*. FEBS Lett. *582*, 503–509.

Rappsilber, J., Mann, M., and Ishihama, Y. (2007). Protocol for micro-purification, enrichment, pre-fractionation and storage of peptides for proteomics using StageTips. Nat. Protoc. *2*, 1896–1906.

Saldanha, A.J. (2004). Java Treeview—extensible visualization of microarray data. Bioinforma. Oxf. Engl. *20*, 3246–3248.

Sathe, L., Bolinger, C., Mannan, M.A., Dever, T.E., and Dey, M. (2015). Evidence that base-pairing interaction between intron and mRNA leader sequences inhibits initiation of HAC1 mRNA translation in yeast. J. Biol. Chem. *290*, 21821–21832.

Schuldiner, M., and Weissman, J.S. (2013). The contribution of systematic approaches to characterizing the proteins and functions of the endoplasmic reticulum. Cold Spring Harb. Perspect. Biol. *5*, a013284.

Sehgal, A., Hughes, B.T., and Espenshade, P.J. (2008). Oxygen-dependent, alternative promoter controls translation of tco1 + in fission yeast. Nucleic Acids Res. *36*, 2024–2031.

Séraphin, B. (1992). The HIT protein family: a new family of proteins present in prokaryotes, yeast and mammals. DNA Seq. *3*, 177–179.

Sidrauski, C., Cox, J.S., and Walter, P. (1996). tRNA ligase is required for regulated mRNA splicing in the unfolded protein response. Cell *87*, 405–413.

Titov, D.V., Cracan, V., Goodman, R.P., Peng, J., Grabarek, Z., and Mootha, V.K. (2016). Complementation of mitochondrial electron transport chain by manipulation of the NAD+/NADH ratio. Science *352*, 231–235.

Travers, K.J., Patil, C.K., Wodicka, L., Lockhart, D.J., Weissman, J.S., and Walter, P. (2000). Functional and genomic analyses reveal an essential coordination between the unfolded protein response and ER-associated degradation. Cell *101*, 249–258.

Tresenrider, A., and Ünal, E. (2018). One-two punch mechanism of gene repression: a fresh perspective on gene regulation. Curr. Genet. *64*, 581–588.

Vander Heiden, M.G., Cantley, L.C., and Thompson, C.B. (2009). Understanding the Warburg effect: the metabolic requirements of cell proliferation. Science *324*, 1029–1033.

Walter, P., and Ron, D. (2011). The unfolded protein response: from stress pathway to homeostatic regulation. Science *334*, 1081–1086.

Warburg, O. (1956). On the origin of cancer cells. Science *123*, 309–314.

Wenger, C.D., Lee, M.V., Hebert, A.S., McAlister, G.C., Phanstiel, D.H., Westphall, M.S., and Coon, J.J. (2011). Gas-phase purification enables accurate, multiplexed proteome quantification with isobaric tagging. Nat. Methods *8*, 933–935.

STAR★METHODS

KEY RESOURCES TABLE

REAGENT or RESOURCE	SOURCE	IDENTIFIER
Antibodies		
Mouse anti-V5	Invitrogen	Cat#46-0705; RRID: AB_2556564
Rat anti-tubulin	Serotec	Cat#MCA78G; RRID: AB_325005
Rabbit anti-Kar2	Mark Rose	N/A
Mouse anti-GFP	Clontech	Cat#632381; RRID: AB_2313808
Goat anti-rat 680	LI-COR	Cat#926-68076; RRID: AB_10956590
Goat anti-mouse 800	LI-COR	Cat#926-32210; RRID: AB_621842
Goat anti-rabbit 800	LI-COR	Cat#926-32211; RRID: AB_621843
Chemicals, Peptides, and Recombinant Proteins		
Phosphatase inhibitor cocktail 2	Sigma	Cat#P5726
Phosphatase inhibitor cocktail 3	Sigma	Cat#P0044
RNase I	Ambion	Cat#AM2294
PNK	NEB	Cat#M0201
PolyA polymerase	NEB	Cat#M0276
Dynabeads MyOne Streptavidin C1	Invitrogen	Cat#65002
Circ ligase	Epicenter	Cat#CL4115K
Superscript III	Invitrogen	Cat#18080044
Phusion polymerase	NEB	Cat#M0530
DynaBeads Oligo-dT	Ambion	Cat#61005
Aprotinin	Sigma	Cat#A6106
Leupeptin	Sigma	Cat#L5793
PMSF	Sigma	Cat#78830
Ultrahyb buffer	Invitrogen	Cat#AM8669
T7 Maxiscript kit	Invitrogen	Cat#AM1312
Sonicated salmon sperm DNA	Agilent	Cat#201190-81
Auxin	Sigma	Cat#12886
IP6	Sigma	Cat#P5681
IP6	Santa Cruz Biotechnology	Cat#sc253276
Tunicamycin	Calbiochem	Cat#504570
Tunicamycin	Calbiochem	Cat#654380
Glyoxal	Sigma	Cat#128465
Hybond-N+ membrane	GE Healthcare	Cat#RPN203B
UTP, alpha P32	PerkinElmer	Cat# BLU507X250UC
Q5 mutagenesis kit	NEB	Cat#E0554S
AflII	NEB	Cat#R0520S
PmeI	NEB	Cat#R0560S
cOmplete mini, EDTA free protease inhibitor cocktail	Roche	Cat#29384100
Acid-washed glass beads	Sigma	Cat#G8772
Poly-L-lysine	Sigma	Cat#P8920
D_3N^{15} Serine	Cambridge isotopes	Cat# DNLM-6863-PK
Luna-5mm NH_2 column	Phenomenex	Cat# 00B-4378-E0
Critical Commercial Assays		
Seahorse XFe96 FluxPak	Agilent	Cat#102601-100

(*Continued on next page*)

Continued

REAGENT or RESOURCE	SOURCE	IDENTIFIER
Deposited Data		
Sequencing	NCBI	GSE115366
Protein mass spectrometry	MassIVE	MSV000082454
Experimental Models: Organisms/Strains		
BrÜn 13 (*MATa*, wild-type)	Brar-Ünal lab	N/A
BrÜn 15 (*MATa/α*, wild-type)	Brar-Ünal lab	N/A
BrÜn 1362 (*MATa/α*, wild-type)	Brar-Ünal lab	N/A
BrÜn 2781 (*MATa/α*, *pet100*::*KanMX*)	This paper	N/A
BrÜn 4431 (*MATa/α*, *hac1*::*NatMX*, *hac1*::*KanMX*)	This paper	N/A
BrÜn 10353 (*MATα*, *hac1*::*NatMX*, *leu2*::*pHAC1-3V5-IAA7-HAC1*::*LEU2*)	This paper	N/A
BrÜn 10532 (*MATa/α*, *hac1*::*NatMX*, *leu2*::*pHAC1-3V5-IAA7-HAC1*::*LEU2*)	This paper	N/A
BrÜn 10744 (*MATa/α*, *hac1*::*NatMX*, *leu2*::*pHAC1-3V5-IAA7-HAC1*::*LEU2*, *his3*::*pCUP1-osTIR1*::*HIS3*)	This paper	N/A
BrÜn 10778 (*MATa*, *hnt1*::*HNT1-3V5*::*KanMX*)	This paper	N/A
BrÜn 10781 (*MATa*, *cox20*::*COX20-3V5*::*KanMX*)	This paper	N/A
BrÜn 10924 (*MATa*, *hac1*::*NatMX*, *leu2*::*pHAC1-3V5-IAA7-HAC1*::*LEU2*, *his3*::*pCUP1-osTIR1*::*HIS3*, *hnt1*::*HNT1-3V5*::*KanMX*)	This paper	N/A
BrÜn 10925 (*MATa*, *hac1*::*NatMX*, *leu2*::*pHAC1-3V5-IAA7-HAC1*::*LEU2*, *hnt1*::*HNT1-3V5*::*KanMX*)	This paper	N/A
BrÜn 10929 (*MATa*, *hac1*::*NatMX*, *leu2*::*pHAC1-3V5-IAA7-HAC1*::*LEU2*, *his3*::*pCUP1-osTIR1*::*HIS3*, *cox20*::*COX20-3V5*::*KanMX*)	This paper	N/A
BrÜn 11133 (*MATa*, *hac1*::*NatMX*, *leu2*::*pHAC1-3V5-IAA7-HAC1*::*LEU2*, *cox20*::*COX20-3V5*::*KanMX*)	This paper	N/A
BrÜn 15924 (*MATa/α*, *ire1*::*NatMX*, *ire1*::*KanMX*)	This paper	N/A
BrÜn 15968 (*MATa*, *trp1*::*pHNT1-GFP*::*TRP1*)	This paper	N/A
BrÜn 16374 (*MATa*, *trp1*::*pHNT1ΔUPRE2-GFP*::*TRP1*)	This paper	N/A
Oligonucleotides		
oCJ200-oligoDT	Table S7	N/A
asDNA-1b	Table S7	N/A
asDNA-2b	Table S7	N/A
asDNA-3b	Table S7	N/A
oNTI231	Table S7	N/A
Index primers: aatgatacggcgaccaccgagatcggaagagcacacgtctgaactccagtcac-barcode-cgacaggttcagagttc (6 base barcodes)	Table S7	N/A
Oligos for northern blotting probes (see Table S7)	Table S7	N/A
Recombinant DNA		
pÜB1073 (*pHAC1-3V5-IAA7-HAC1*)	This paper	N/A
pÜB1397 (*pHNT1-GFP*)	This paper	N/A
pÜB1406 (*pHNT1ΔUPRE2-GFP*)	This paper	N/A
Software and Algorithms		
Bowtie2	Langmead and Salzberg, 2012	http://bowtie-bio.sourceforge.net/bowtie2/index.shtml
Cluster 3.0	De Hoon et al., 2004	http://bonsai.hgc.jp/~mdehoon/software/cluster/software.htm
MochiView	Homann and Johnson, 2010	http://www.johnsonlab.ucsf.edu/mochi/
Treeview	Saldanha, 2004	http://jtreeview.sourceforge.net/
ImageStudio Lite Software	LI-COR	https://www.licor.com/bio/products/software/image_studio_lite/index.html

(*Continued on next page*)

Continued		
REAGENT or RESOURCE	SOURCE	IDENTIFIER
GraphPad Prism	GraphPad Software	https://www.graphpad.com/scientific-software/prism/
MassHunter Workstation LC/MS Data Acquisition	Agilent	Version B.05.00
MassHunter Workstation Qualitative Analysis	Agilent	Version B.06.00
Other		
Seahorse Analyzer	Agilent	XFe96 model
QQQ LC-MS/MS	Agilent	6430 model

CONTACT FOR REAGENT AND RESOURCE SHARING

Further information and requests for resources and reagents should be directed to and will be fulfilled by the Lead Contact, Gloria Ann Brar (gabrar@berkeley.edu).

EXPERIMENTAL MODEL AND SUBJECT DETAILS

Yeast Strain Construction

All experiments were performed using *Saccharomyces cerevisiae* strains of the SK1 background.

Gene Deletion Strains

Deletions were created by one-step gene deletion, as described in (Longtine et al., 1998).

AID-HAC1 *Strain*

Construction of this strain required deleting endogenous *HAC1* and replacing it ectopically with an auxin-inducible degron (AID)-tagged version. We ensured that the promoter, intron, and UTRs, which are all required for proper regulation of *HAC1*, were not disrupted in this construct [Figure 3A; (Aragón et al., 2009; Bowring and Llewellyn, 2001; Ogawa and Mori, 2004; Sathe et al., 2015)]. To build the allele, we cloned 507bp upstream of the *HAC1* ORF in front of a 3V5 tag, followed by the IAA7 degron, the *HAC1* ORF, and 844bp downstream of the *HAC1* stop codon. The entire construct was cloned into a *LEU2* integrating vector (resulting in plasmid pÜB1073) and the AflII (NEB) digestion product was subsequently transformed into a strain heterozygous for *hac1Δ*. Following sporulation, haploids were chosen that carried the *AID-HAC1* allele as their sole source of Hac1.

HNT1-3V5 and COX20-3V5 Strains

A c-terminal *3V5* tag, marked by a G418 resistance cassette, was integrated into the endogenous locus, replacing the stop codon.

GFP Reporter Strains

For *pHNT1-GFP*, *pHNT1* (-600 to +42) was cloned ahead of a ubiquitin-GFP fusion, followed by the *Candida albicans ADH1* terminator, resulting in pÜB1397. For *pHNT1ΔUPRE2-GFP*, the first five of the six bp in the UPRE2 motif starting at -284 were deleted from pÜB1397 via Q5 mutagenesis, resulting in pÜB1406. Constructs were integrated at the *TRP1* locus via transformation with the PmeI (NEB) digestion product of the relevant plasmid.

Yeast Growth Conditions

Strains were grown in YEPD(2%) at 30C, with shaking. Plate-based growth assays were carried out on YEPD(4%) plates at 30C.

METHOD DETAILS

Sample Collection for Sequencing Experiments

WT/ hac1Δ

BrÜn 1362 (WT) and 4431(*hac1Δ*) were inoculated into YEPD and grown at 30C overnight, then diluted to OD_{600}0.05 in YEPD. After approximately 2 doublings, cultures were split into 3 subcultures. Per strain, a first subculture received no treatment, a second was treated with 5mM DTT, and a third was treated with 2μg/mL Tm (Calbiochem). After 1 hr, 500 mL samples were collected as in (Brar et al., 2012), using 30 sec cycloheximide treatment, filtration, and flash freezing (in 2 portions - ~90% for ribosome profiling and ~10% for mRNA-sequencing). 2mL flash frozen buffer (20mM TRIS pH8, 140mM KCl, 1.5mM $MgCl_2$, 100μg/mL cycloheximide, 1% Triton X-100) was added to each ribosome profiling aliquot. Samples were lysed via Retsch mixermilling (6X 3 min, 15 Hz). Resulting powder was thawed and spun at 4C for 5 min, 3,000 x g. Supernatant was removed and cleared at 4C for 10 min, 20,000 x g.

AID-HAC1

BrÜn 10532 (*AID-HAC1 -TIR1*) and 10744(*AID-HAC1 +TIR1*) were inoculated into YEPD and grown at 30C overnight, then diluted to OD_{600}0.05 in YEPD. After approximately 2 doublings, cultures were split into 2 subcultures. Per strain, one subculture was treated with 500μM auxin (Sigma) and 4μM IP_6 (Sigma) and the other with equivalent volumes of DMSO and water. After 15 min, the subcultures treated with auxin and IP6 were further split into 2 subcultures. Per strain, 1 auxin-pre-treated culture was not treated further

(+auxin), and 1 was treated with 5mM DTT (+auxin +DTT). For each strain, the DMSO pre-treated subculture was treated with 5mM DTT (+DTT +vehicle). After 1 hr, 500 mL per culture was harvested identically as in the WT/*hac1Δ* experiment, except the buffer was supplemented with 2μg/mL Aprotinin (Sigma), 10μg/mL Leupeptin (Sigma), 1 mM PMSF (Sigma), 1:100 PIC2 (Sigma), and 1:100 PIC3 (Sigma). After 1 additional hr, a second 500 mL sample was harvested from each culture. Extract was prepared as in the WT/*hac1Δ* experiment, and identical extract was used for ribosome profiling and mass spectrometry.

Additional Sample Collection for Protein/RNA

WT/hac1Δ Transcript Comparisons

One biological replicate was derived from total RNA prepared for the sequencing experiment described above. An additional replicate was collected similarly, except was harvested by filtration without the addition of cycloheximide.

WT/ ire1Δ Transcript Comparisons

Two biological replicates were collected as follows. BrÜn 15 (WT) and 15924 (*ire1Δ*) were inoculated into YEPD and grown at 30C overnight, then diluted to OD_{600}0.05 in YEPD. After approximately 2 doublings, cultures were split into 3 subcultures. Per strain, a first subculture received no treatment, a second was treated with 5mM DTT, and a third was treated with 2μg/mL Tm (Calbiochem). Samples were harvested at the indicated times by filtration.

Additional AID-HAC1 Transcript Comparisons

For cases where cells were pre-treated with auxin and subsequently treated with DTT, one biological replicate was derived from total RNA prepared for the sequencing experiment above. An additional replicate was collected similarly, except was directly harvested by filtration without the addition of cycloheximide. For analysis of AID-Hac1 protein levels in these experiments, 3 biological replicates were collected similarly except 2.5 OD units were harvested at each time point and treated with 5% trichloroacetic acid (TCA).

For cases where cells were pre-treated with DTT and subsequently treated with auxin, 2 biological replicates were collected as follows. BrÜn 10532 (*AID-HAC1 -TIR1*) and 10744(*AID-HAC1 +TIR1*) were inoculated into YEPD and grown at 30C overnight, then diluted to OD_{600}0.05 in YEPD. After approximately 2 doublings, the BrÜn 10744 culture was split into 2 subcultures. BrÜn 10532 and one of the BrÜn 10744 subcultures were treated with 5 mM DTT, while the other BrÜn 10744 subculture remained untreated. After 45 min, samples from each culture were collected by filtration. Both DTT-treated cultures were then treated with 500μM auxin (Sigma) and 4μM IP_6 (Sigma/Santa Cruz Biotechnology), while the untreated culture was treated with DMSO. Additional samples were collected by filtration at the indicated times. For analysis of Kar2 protein levels in these experiments, 3 biological replicates were collected similarly except 2.5 OD units were harvested at each time point and treated with 5% TCA.

Evaluation of HNT1 and COX20 Expression

For evaluation of Hnt1 and Cox20 protein levels upon DTT or Tm treatment (Figures 2G, 2I, 5G, 5I), BrÜn 10778 (*HNT1-3V5*) and 10781 (*COX20-3V5*) were harvested as follows. The appropriate strain was inoculated into YEPD and grown at 30C overnight, then diluted to OD_{600}0.05 in YEPD. After ~2 doublings, 2.5 OD units were collected and treated with 5% TCA, and cultures were subsequently treated with either DTT or Tm. Additional samples (2.5 OD units each time) were taken at the indicated times. Three full biological replicates were harvested for each condition. For similar experiments in the *AID-HAC1* background, BrÜn 10924 and 10925 were used for Hnt1 analysis, and BrÜn 10929 and 11133 were used for Cox20 analysis. Collection was the same, except that cultures were pre-treated for 15 min with 500μM auxin (Sigma) and 4μM IP_6 (Sigma) prior to initial sample collection and 5mM DTT treatment. Additionally, approximately 20mL per culture was collected at each time point and used for downstream RNA applications.

Evaluation of GFP Reporter Expression

For evaluation of *GFP* transcript levels, BrÜn 15968 (*pHNT1-GFP*) and 16374 (*pHNT1ΔUPRE2-GFP*) were inoculated into YEPD and grown at 30C overnight, then diluted to OD_{600}0.05 in YEPD. After ~2 doublings, cultures were treated with 5mM DTT. Following 90 min treatment, samples were harvested by filtration and flash-frozen for total RNA isolation. Two biological replicates were harvested for each condition.

For evaluation of GFP protein levels (Figure 2M), BrÜn 15968 (*pHNT1-GFP*) and 16374 (*pHNT1ΔUPRE2-GFP*) were inoculated into YEPD and grown at 30C overnight, then diluted to OD_{600}0.05 in YEPD. After ~2 doublings, 2.5 OD units were collected and treated with 5% TCA, and cultures were subsequently treated with 5mM DTT. Additional samples (2.5 OD units each time) were taken at the indicated times. Three biological replicates were harvested for each condition.

Growth Curves

For Figure 3B, growth curve was performed as follows: BrÜn 13 (WT), BrÜn 4431 (*hac1Δ*), and BrÜn 10353 (*AID-HAC1*) were inoculated into YEPD and grown at 30C overnight, then diluted to OD_{600}0.05 in YEPD. After 7 hr, cultures were back-diluted to OD_{600}0.15 in YEPD. In a 96-well plate, 150μL cells were treated in triplicate with 2.5mM DTT. Cultures were grown overnight in a 30C, shaking plate reader (Tecan Infinite M1000), with absorbance at 600nm measurements taken every 15 min. Absorbance readings in Figure 3B represent averaged values across triplicate wells.

For Figures 6E and 6F, growth curves were performed as follows: BrÜn 15 (WT) and BrÜn 2781 (*pet100Δ*) were inoculated into YEPD and grown at 30C overnight, then diluted to OD_{600}0.05. After ~2 doublings, cultures were split into 2 subcultures, one of which remained untreated and one of which was treated with 5mM DTT. OD_{600} readings were taken every hr. OD_{600} values in Figures 6E and 6F are normalized to the exact OD_{600} reading just before treatment and represent average fold change from starting OD_{600} across 3 biological replicates.

Plate-Based Growth Assays

BrÜn 15 (WT) and BrÜn 2781(*pet100Δ*) were inoculated into YEPD and grown at 30C overnight, then diluted to OD_{600}0.2 in YEPD. Approximately 4.5 hr later, cultures were diluted to OD_{600}0.1 in water. Samples were briefly sonicated to prevent clumping, and 5-fold dilutions were prepared in water. 3 μL of each dilution were plated on YEPD (4%) containing 0μg, 0.5μg or 0.75μg/mL Tm. Plates were imaged after 2 nights at 30C.

Northern Blotting

All RNA was isolated using the hot acid phenol method. 8-10μg of total RNA was denatured in glyoxal mix [1M glyoxal (Sigma), 50% DMSO, 10mM $NaPO_4$ pH 6.8] for 10 min at 70C. Denatured samples were loaded onto a 1.1% agarose gel, separated at 116V for 3 hr, and transferred overnight to a nylon membrane [Hybond-N+ (GE)]. Following UV crosslinking and methylene blue staining, the membrane was blocked at 68C for at least 45 min with Ultrahyb buffer (Invitrogen) supplemented with boiled sonicated salmon sperm DNA (Agilent). All probe templates were generated by PCR (primers in Table S7) of WT yeast genomic DNA, except the *GFP* probe template, which was generated by amplification from a *GFP*-containing plasmid. The probe was *in vitro* transcribed [MaxiScript T7 Kit (Invitrogen)] using all kit components, except cold UTP was replaced with alpha-P32 labeled UTP (PerkinElmer). The blot was incubated with the hot probe at 68C overnight, and subsequently washed for 2X 5 min at RT with low stringency wash buffer (2X SSC, 0.1% SDS) and 2X 15 min at 68C with high stringency wash buffer (0.1X SSC, 0.1% SDS). Typhoon phosphor-imaging was used for visualization. For each transcript probed, at least 2 biological replicates were performed and sizing was confirmed on a sample blot with ladders (Figures S7E–S7G) and, more routinely, by comparison to rRNA bands. In our experience, likely due to their highly stable structural features, rRNA (2.0 kB and 3.8 kB) species tend to migrate slightly faster than would be expected for mRNAs (for example, Figures S7I and S7J), making all of our size comparisons approximate.

Western Blotting

Western blotting was performed using a TCA protocol, similar to that described by (Chen et al., 2017). Briefly, 2.5 OD units of culture were treated with 5% TCA at 4C for at least 10 min. Samples were then washed with 1mL acetone. Acetone was aspirated and pellets were dried overnight at RT. Lysates were made by adding 100μl protein lysis buffer [50mM TE, 3mM DTT, 1.1mM PMSF (Sigma), 1μM pepstatin A, 1X protease inhibitor cocktail (Roche)] and 1 volume acid-washed glass beads (Sigma), and bead-beating for 5 min at RT. 3X SDS loading buffer was added and samples were boiled for 5 min. Beads were pelleted by centrifugation and 5μL supernatant was loaded onto 4-12% Bis-Tris polyacrylamide gels. Following electrophoresis, proteins were transferred using a semi-dry transfer apparatus (Trans-Blot Turbo, BioRad). The following antibodies were used: mouse anti-V5 (Invitrogen, 1:2,000), rat anti-tubulin (Serotec, 1:10,000), rabbit anti-Kar2 (gift of Mark Rose, 1:100,000), mouse anti-GFP (Clontech, 1:500), goat anti-rat680 (LI-COR, 1:15,000), goat anti-mouse800 (LI-COR, 1:15,000), goat anti-rabbit 800 (LI-COR, 1:15,000). Example uncropped blots for all proteins examined in this work are shown in Figure S7 (L-P) to demonstrate sizing relative to ladder.

Ribosome Profiling Library Generation

Ribosome profiling libraries were prepared as described as in (Cheng et al., 2018). Briefly, footprints were prepared by treating extract with 15U RNAse I (Ambion) per A_{260} unit for 1 hr at RT. Monosomes were isolated by sucrose gradient (10-50%). RNA was isolated by the hot acid phenol method. Samples were size-selected (by PAGE), dephosphorylated [PNK (NEB)], polyA-tailed [PolyA polymerase (NEB) with oCJ200-oligodT], subtracted of rRNA [MyOne Streptavidin C1 dynabeads (Invitrogen) with asDNA1b-3b], and reverse transcribed [Superscript III (Invitrogen)]. RT products were size-selected (by PAGE), circularized [Circ ligase (Epicenter)], and PCR amplified [Phusion polymerase (NEB) with oNTI231and index primers]. Following gel purification, libraries were sequenced using standard Illumina oligos.

mRNA-Sequencing Library Generation

mRNA-sequencing libraries were prepared as described in (Cheng et al., 2018). Briefly, RNA was extracted by the hot acid phenol method and was polyA-selected [oligodT Dynabeads (Ambion)]. Samples were alkaline fragmented, then size-selected (by PAGE) and subsequently dephosphorylated, polyA-tailed, and reverse transcribed as for the ribosome profiling libraries. RT products were similarly size-selected, circularized, and PCR amplified. Following gel purification, libraries were sequenced using standard Illumina oligos.

Sequencing

All sequencing was done at the UC-Berkeley Vincent J. Coates QB3 Sequencing Facility. Libraries were sequenced on an Illumina HiSeq 2500, 50SRR, with multiplexing.

Metabolomic Profiling

Samples were harvested as follows: For Figure S6A, BrÜn 10532 (*AID-HAC1 –TIR1*) and 10744 (*AID-HAC1 +TIR1*) were inoculated into YEPD and grown at 30C overnight, then diluted to OD_{600}0.05 in YEPD. After approximately 2.5 doublings, cultures were treated with 500μM auxin (Sigma) and 4μM IP_6 (Sigma). After 15 min, cultures were split into subcultures. Per strain, one subculture was not treated further (+auxin), and one was treated with 2μg/mL Tm (Calbiochem) (+auxin +Tm). After 2 hr, cultures were harvested by centrifugation (4C, 2,000 x g, 1 min), washed in cold water (4C, 15,000 x g, 30 sec), and flash frozen in ~30mg aliquots. Five technical

replicates were collected per condition. For Figure 6A, BrÜn 15 (WT) was used, except without the addition of auxin/IP6 and 6 technical replicates were collected per condition.

For both experiments, metabolomic analyses were performed as reported previously (Louie et al., 2016). Briefly, frozen cell pellets were resuspended with 150μL 40:40:20 acetonitrile/methanol/water containing 10nmoles D_3N^{15} serine internal standard (Cambridge isotopes). Samples were vortexed thoroughly for 30 sec and bath sonicated for 15 sec before centrifugation at 21,000 x g for 10 min. Supernatant was collected and frozen at −80° C until analysis. 20 μL of supernatant was analyzed by single-reaction monitoring (SRM)-based targeted LC-MS/MS. Separation of metabolites was performed by normal-phase chromatography using a Luna-5 mm NH2 column (50 mm x 4.60 mm, Phenomenex). Mobile phases were run as follows: Buffer A, acetonitrile; Buffer B, 95:5 water/acetonitrile with 0.1% formic acid or 0.2% ammonium hydroxide with 50 mM ammonium acetate for positive and negative ionization modes, respectively. Flow rate began at 0.2 mL/min for 2 min, followed by a gradient starting at 0% B and increasing linearly to 100% B over the course of 13 min with a flow rate of 0.7 mL/min, followed by an isocratic gradient of 100% B for 10 min with a flow rate of 0.7mL/min before equilibrating for 5 min at 0% B with a flow rate of 0.7 mL/min. MS analysis was performed using an electrospray ionization (ESI) source on an Agilent 6430 QQQ LC-MS/MS. Capillary voltage was 3.0 kV, fragmentor voltage was 100 V, drying gas temperature 350° C, drying gas flow rate was 10 L/min, and the nebulizer pressure was 35 psi. Representative metabolites were quantified by SRM of the transitions from precursor to product ions at associated collision energies. Data was analyzed by calculating area under the curve using Agilent Qualitative Analysis software.

Oxygen Consumption Assay

Except for materials needed for yeast cultures, all steps were carried out using components from a Seahorse Extracellular FluxPak (Agilent).

Preparation of Cartridge

A Seahorse Extracellular Flux cartridge was hydrated with 200μl water per well overnight at 30C. Approximately 90 min prior to taking basal OCR measurements, water was removed and replaced with 200μl pre-warmed XF Calibrant solution.

Preparation of Cell Culture Plate

Wells were coated with 20μl 0.1mg/mL poly-L-lysine (Sigma) for 10 min at RT. Poly-L-lysine was then removed and the plate allowed to dry before adding cells. Cells were grown and plated as follows. BrÜn 15 (WT) was inoculated into YEPD and grown at 30C overnight, then diluted to OD_{600}0.05 in YEPD. After ~2 doublings, cells were treated with 2μg/mL Tm (Calbiochem). This culture was used for the 6.5 hr Tm treatment samples. After 4.5 hr, an additional OD_{600}0.05 culture was started from the overnight inoculation, and after ~2 doublings, cells were treated with 2μg/mL Tm (Calbiochem) or vehicle. These cultures were used for the 2 hr Tm treatment samples and the control samples, respectively. After 6 hr and 1.5 hr, respectively, 0.3 OD units centrifuged at 1,500 x g, 2 min, RT. Cells were resuspended in 2 mL and then diluted 1:6 in fresh media (supplemented with Tm as appropriate). 180ul was added to each of 12 wells per condition. The plate was spun at 500 x g for 3 min at RT and then placed at 30C for 30 min. Immediately before OCR measurements, the plate was spun again as before.

OCR Measurements

Following initial calibration, basal OCR was measured using a 2 min mix, 2 min measure protocol. Measurements, normalized to OD at the end of the assay, are reported in Figure 6D.

Mass Spectrometry

TMT-Labeling and Sample Fractionation

Proteins were precipitated by adding −20°C cold acetone to the lysate (acetone to eluate ratio 10:1) and overnight incubation at −20°C. The proteins were pelleted by centrifugation at 20000xg for 15 min at 4°C. The supernatant was discarded and the pellet was left to dry by evaporation. The protein pellet was reconstituted in 100μl urea buffer (8M Urea, 75mM NaCl, 50mM Tris/HCl pH 8.0, 1mM EDTA), and protein concentrations were determined by BCA assay (Pierce). Fifteen μg of total protein per sample were processed further. Disulfide bonds were reduced with 5mM DTT and cysteines were subsequently alkylated with 10mM iodoacetamide. Samples were diluted 1:4 with 50mM Tris/HCl (pH 8.0) and sequencing grade modified trypsin (Promega) was added in an enzyme-to-substrate ratio of 1:50. After 16hr of digestion, samples were acidified with 1% formic acid (final concentration). Tryptic peptides were desalted on C18 StageTips according to (Rappsilber et al., 2007) and evaporated to dryness in a vacuum concentrator. Desalted peptides were labeled with the TMT11plex mass tag labeling reagent according to the manufacturer's instructions (Thermo Scientific) with small modifications. Briefly, 0.2units of TMT10plex reagent was used per 15μg of sample. Peptides were dissolved in 30μl of 50mM Hepes pH 8.5 solution and the TMT10plex reagent was added in 12.3μl of MeCN. After 1hr incubation, the reaction was stopped with 2.5μl 5% Hydroxylamine for 15min at 25°C. Differentially labeled peptides were mixed for each replicate (A-L were labeled with 126C, 127N, 127C, 128N, 128C, 129N, 129C, 130N, 130C, 131N, 131C, respectively) and subsequently desalted on C18 StageTips (Rappsilber et al., 2007) and evaporated to dryness in a vacuum concentrator.

The peptide mixtures were fractionated by Strong Cation Exchange (SCX) using StageTips as previously described (Rappsilber et al., 2007) with slight modifications. Briefly, one StageTip was prepared per sample by three SCX discs (3M, #2251) topped with two C18 discs (3M, #2215). The packed StageTips were first washed with 100μl methanol and then with 100μl 80% acetonitrile and 0.2% formic acid. Afterwards, they were equilibrated by 100μl 0.2% formic acid and the sample was loaded onto the discs. The sample was transeluted from the C18 discs to the SCX discs by applying 100μl 80% acetonitrile; 0.2% formic acid, which was followed by 3 stepwise elutions and collections of the peptide mix from the SCX discs. The first fraction was eluted

with 50μl 50mM NH_4AcO; 20% MeCN (pH ~7.2), the second with 50μl 50mM NH_4HCO_3; 20% MeCN (pH ~8.5) and the sixth with 50μl 0.1% NH_4OH; 20% MeCN (pH ~9.5). 200μl of 0.2% acetic acid was added to each of the three fractions, and they were subsequently desalted on C18 StageTips as previously described (Rappsilber et al., 2007) and evaporated to dryness in a vacuum concentrator. Peptides were reconstituted in 10μl 0.2% formic acid. Both the unfractionated samples plus the fractionated, less complex samples were then analyzed by LC-MS/MS on a Q-Exactive HF was performed as previously described (Keshishian et al., 2015).

Approximately 1μg of total peptides was analyzed on an Eksigent nanoLC-415 HPLC system (Sciex) coupled via a 25cm C18 column (inner diameter of 100μm, packed in-house with 2.4μm ReproSil-Pur C18-AQ medium, Dr. Maisch GmbH) to a benchtop Orbitrap Q Exactive HF mass spectrometer (Thermo Fisher Scientific). Peptides were separated at a flow rate of 200nL/min with a linear 106min gradient from 2% to 25% solvent B (100% acetonitrile, 0.1% formic acid), followed by a linear 5min gradient from 25 to 85% solvent B. Each sample was run for 170min, including sample loading and column equilibration times. Data was acquired in data dependent mode using Xcalibur 2.8 software. MS1 Spectra were measured with a resolution of 60,000, an AGC target of 3E6 and a mass range from 375 to 2000m/z. Up to 15 MS2 spectra per duty cycle were triggered at a resolution of 60,000, an AGC target of 2E5, an isolation window of 1.6 m/z and a normalized collision energy of 36.

Label-Free Quantification

In order to validate the TMT-based quantification results, we performed proteomics based on LFQ, which does the quantification on the MS1 level, instead of the MS2 level, and does not allow multiplexing as does TMT labeling. Therefore, different systematic biases are introduced by LFQ based proteomics than by TMT based proteomics, and it serves as a quite stringent test to our deep proteome quantification results obtained by our TMT based approach. We quantified all 11 matched samples.

Proteins were precipitated by adding −20°C cold acetone to the lysate (acetone to eluate ratio 10:1) and overnight incubation at −20°C. The proteins were pelleted by centrifugation at 20000xg for 15min at 4°C. The supernatant was discarded and the pellet was left to dry by evaporation. The protein pellet was reconstituted in 100μl urea buffer (8M Urea, 75mM NaCl, 50mM Tris/HCl pH 8.0, 1mM EDTA) and protein concentrations were determined by BCA assay (Pierce). 20μg of total protein per sample were processed further. Disulfide bonds were reduced with 5mM DTT and cysteines were subsequently alkylated with 10mM iodoacetamide. Samples were diluted 1:4 with 50mM Tris/HCl (pH 8.0) and sequencing grade modified trypsin (Promega) was added in an enzyme-to-substrate ratio of 1:50. After 16h of digestion, samples were acidified with 1% formic acid (final concentration). Tryptic peptides were desalted on C18 StageTips according to (Rappsilber et al., 2007) and evaporated to dryness in a vacuum concentrator. Desalted peptides were reconstituted in Buffer A (0.2% Formic acid).

LC-MS/MS analysis was performed on a Q-Exactive HF. Approximately 1μg of total peptides were analyzed on an Eksigent nanoLC-415 HPLC system (Sciex) coupled via a 25cm C18 column (inner diameter 100μm packed in-house with 2.4μm ReproSil-Pur C18-AQ medium, Dr. Maisch GmbH) to a benchtop Orbitrap Q Exactive HF mass spectrometer (Thermo Fisher Scientific). Peptides were separated at a flow rate of 200nL/min with a linear 106min gradient from 2% to 25% solvent B (100% acetonitrile, 0.1% formic acid), followed by a linear 5min gradient from 25 to 85% solvent B. Each sample was run for 170min, including sample loading and column equilibration times. Data was acquired in data dependent mode using Xcalibur 2.8 software. MS1 Spectra were measured with a resolution of 60,000, an AGC target of 3E6 and a mass range from 375 to 2000m/z. Up to 15 MS2 spectra per duty cycle were triggered at a resolution of 15,000, an AGC target of 2E5, an isolation window of 1.6 m/z and a normalized collision energy of 27.

QUANTIFICATION AND STATISTICAL ANALYSES

Sequence Alignments and Analysis

Performed as described in (Cheng et al., 2018), we observed the high technical and biological reproducibility that our lab typically observes using ribosome profiling and mRNA-sequencing. Plots are provided (Figure S7) that exemplify this reproducibility. In the cases analyzed, we compared samples that should be biologically similar and that were harvested to provide additional controls within the experiment presented in Figure 4A. Alignments were done using bowtie2 (Langmead and Salzberg, 2012). Genome browser analysis was done using Mochiview (Homann and Johnson, 2010). Cluster analysis and visualization were done using Cluster 3.0 and Java Treeview, respectively (De Hoon et al., 2004; Saldanha, 2004).

LUTI Identification

mRNA-seq and ribosome profiling data for WT and *hac1Δ* cells, with either no treatment or treatment with DTT or Tm, as described above, were analyzed by genome browser (Mochiview). All annotated yeast genes were inspected visually for evidence of an alternate, 5′ extended transcript with translated uORFs that was Hac1- and UPR^{ER}-dependent. This approach was enabled by the simple transcript structures of most budding yeast genes. Of the ~30 candidates found by this approach, 19 showed an associated Hac1-dependent decrease in TE and were defined as candidate LUTIs. This set of 19 was reevaluated one-by-one in the AID-Hac1 experiment to determine if these hallmarks remained strong. In 15 cases, this was true, and these genes are presented in Table 1. Note that a major caveat of this approach is that it is biased towards analysis of highly expressed mRNAs, as it is much more straightforward in these cases to detect the robust presence of alternate transcripts.

Translation Efficiency Calculations

TE values were obtained as described in (Ingolia et al., 2009). We calculated TE by dividing unfiltered footprint RPKMs by unfiltered mRNA RPKMs, summing reads over each annotated canonical ORF.

Statistical Analyses

Hac1 Target Gene Expression

We analyzed our sequencing and mass spectrometry data to determine if reported Hac1 targets (Travers et al., 2000) displayed the expected trends. In cases where we show changes in transcript or translation levels upon DTT or Tm treatment (Figures 1C, 1D, 4B, S1A, S1B, S4D), we calculated the number of reported Hac1 targets up-regulated upon DTT or Tm treatment (fold-change Y/X > 1). We performed a resampling test (10,000 iterations) by taking subsamples from the overall gene set of size equal to the target gene set and calculating the number of up-regulated genes. P-values were determined from the frequency distribution of the number of up-regulated genes compared to the Hac1 target gene set. In cases where we show differences in transcript or translation levels between cells with and without Hac1 (Figures 1E, S1C, S1D, S4A–S4C, and S4E), we performed identical analyses using the inverse of the fold change (X/Y).

Metabolomics Data

Reported p-values were generated by t-tests.

Oxygen Consumption Data

Reported p-values were generated by a two-tailed Mann-Whitney test.

Western Blot Quantification

Quantification of triplicate biological replicates was performed on raw images in Image Studio Lite (LI-COR). Signal intensity was normalized to that of a tubulin loading control.

Analysis of TMT Mass Spectrometry

All raw data were analyzed with MaxQuant software version 1.6.0.16 (Cox and Mann, 2008) using a UniProt yeast database (release 2014_09, strain ATCC 204508 / S288c), and MS/MS searches were performed with the following parameters: The five mass spec runs were grouped together. TMT11plex labeling on the MS2 level, oxidation of methionine and protein N-terminal acetylation as variable modifications; carbamidomethylation as fixed modification; Trypsin/P as the digestion enzyme; precursor ion mass tolerances of 20 p.p.m. for the first search (used for nonlinear mass re-calibration) and 4.5 p.p.m. for the main search, and a fragment ion mass tolerance of 20 p.p.m. For identification, we applied a maximum FDR of 1% separately on protein and peptide level. We required 1 or more unique/razor peptides for protein identification and a ratio count for each of the 11 TMT channels. This gave us a total of 2577 quantified protein groups.

Finally, we normalized the MaxQuant generated corrected TMT intensities such that at each condition/time point the corrected TMT intensity values added up to exactly 1,000,000; therefore each protein group value can be regarded as a normalized microshare (we did this separately for each TMT channel for all proteins that made our filter cutoff in all the TMT channels).

Note: In order to compare protein group specific intensity values between the TMT quantified samples and our control label free quantified (LFQ) samples, we adjusted the normalization for the TMT data in order to incorporate the MS1 information as well. Each protein group of a TMT labeled sample got its proportional fraction of the MS1 based iBAQ intensities based on its labeling channel specific TMT MS2 intensity relative to the sum of TMT MS2 intensities of all labeled channels for the corresponding protein group. Afterwards we normalized these fractional MS1 iBAQ intensities such that at each condition/time point these intensity values added up to exactly 1,000,000, therefore each protein group value can be regarded as a normalized microshare. These microshare values are then comparable to the normalized microshare iBAQ based intensities from our label free samples (see below).

Analysis of LFQ Mass Spectrometry

All raw data were analyzed with MaxQuant software version 1.6.0.1 (Cox and Mann, 2008) using a UniProt yeast database (release 2014_09, strain ATCC 204508 / S288c), and MS/MS searches were performed with the following parameters: Oxidation of methionine and protein N-terminal acetylation as variable modifications; carbamidomethylation as fixed modification; Trypsin/P as the digestion enzyme; precursor ion mass tolerances of 20 p.p.m. for the first search (used for nonlinear mass re-calibration) and 4.5 p.p.m. for the main search, and a fragment ion mass tolerance of 20 p.p.m. For identification, we applied a maximum FDR of 1% separately on protein and peptide level. "Match between the runs" was activated, as well as the "iBAQ" field. A total of 2475 protein groups was identified by at least 1 or more unique/razor peptides in any of the 11 samples. For any comparison between different samples only protein groups that had been assigned iBAQ values in each of the samples that were used.

Finally, we normalized the MaxQuant generated iBAQ intensities such that at each condition/time point the iBAQ intensity values added up to exactly 1,000,000; therefore each protein group value can be regarded as a normalized microshare (we did this separately for each sample for all proteins that were present in that sample).

DATA AND SOFTWARE AVAILABILITY

All sequencing data can be accessed at NCBI GEO with accession number GSE115366. Mass spectrometry data are available on the MassIVE platform with accession number MSV000082454.